# Modeling, Simulation, and Flight Characteristics of an Aircraft Designed to Fly at 100,000 Feet

Alex G. Sim
NASA Dryden Flight Research Facility, Edwards, California

1991

# NASA

National Aeronautics and
Space Administration

**Dryden Flight Research Facility**
Edwards, California 93523-0273

# CONTENTS

# ABSTRACT

A manned real-time simulation of a conceptual vehicle, the stratoplane, was developed to study problems associated with the flight characteristics of a large, lightweight vehicle. Mathematical models of the aerodynamics, mass properties, and propulsion system were developed in support of the simulation and are presented. The simulation was at first conducted without control augmentation to determine the needs for a control system. The unaugmented flying qualities were dominated by lightly damped dutch roll oscillations. Constant pilot workloads were needed at high altitudes. Control augmentation was investigated using basic feedbacks. For the longitudinal axis, flightpath angle and pitch rate feedback were sufficient to damp the phugoid mode and to provide good flying qualities. In the lateral-directional axis, bank angle, roll rate, and yaw rate feedbacks were sufficient to provide a safe vehicle with acceptable handling qualities. Intentionally stalling the stratoplane to very high angles of attack (deep stall) was investigated as a means to enable safe and rapid descent. It was concluded that the deep-stall maneuver is viable for this class of vehicle.

# INTRODUCTION

At the July 1989 Truckee Conference (Chambers, 1989), representatives of the atmospheric science community affirmed the need for an atmospheric sampling aircraft capable of flight in the stratosphere at a minimum altitude of 100,000 ft. Their mission requirements were for an aircraft to carry a 2500-lb payload for 6000 mi at an altitude of 100,000 ft. Before the conference, a vehicle with similar mission capabilities had been studied by the Lockheed Aircraft Corporation, Burbank, California (Chambers, 1990). The Lockheed vehicle was a twin-engine configuration designed around reciprocating engines integrated with a three-stage turbocharger system. Each engine was to produce 500 hp. In the total vehicle design, the area of high technical risk was the engine and turbocharger development. Two aircraft could be developed and manufactured in approximately 4 years. At the time of the conference, the scientists considered the development time unattractive and lacked sufficient funds for this level of aircraft development.

After the Truckee Conference, the NASA Dryden Flight Research Facility responded to the need for a high-altitude aircraft by continuing to study, advocate, and further develop the aircraft design through in-house and contracted efforts. Engines have been identified that need only to be derated and can be used without extensive development. Also, applicable turbo-machinery hardware have been identified that were originally developed for the Teal Rain (TRX) and its successor, the Condor (Henderson, 1990).

Many configurations have been studied, including variations in the number of engines, span, payload, and unmanned flight. One configuration studied was a manned single-engine stratospheric engine demonstrator vehicle, the stratoplane, and is the topic of this report. The stratoplane is a conceptual design of a large, manned single-engine monoplane created to conduct atmospheric sampling and to validate its engine technology. The vehicle was designed with a gross weight of 11,100 lb, a wing span of 180 ft, and a propeller 30 ft in diameter. Conceptually, this vehicle would be used to validate and refine the propulsion technology before building a full mission vehicle and to conduct missions of lesser payload and range. The stratoplane would have an approximately 1000-lb payload capability and a 3700-nmi range at an altitude of 100,000 ft.

A simulation study was conducted from May through October 1990 to address concerns over the stability, control, and flying qualities of operating a manned stratoplane vehicle. The study was limited to quickly bounding the concerns rather than conducting an indepth analysis. For example, a rigid body model was used for the aerodynamics and specific aerodynamics terms were varied to bound the aeroelastic effects.

The final phase of the study used a real-time manned simulator with a fixed-base generic cockpit similar to the type used in Smith, Schilling, and Wagner, 1989. Mathematical models of the aerodynamics, propulsion system and mass properties were developed to support both the simulation and a linear control analysis. The aerodynamics

model was implemented to very high angles of attack to allow for evaluation of the controlled deep-stall maneuver used in Sim, 1990.

The scope of the control system evaluation was limited to primarily the basic feedback of rates and attitudes. This report documents the models used to build up the simulation, the vehicle flying qualities, and the resulting control system.

## DESIGN CONSIDERATIONS

The primary design of the stratoplane had been established (fig. 1) before undertaking this study of flight characteristics. However, it is of interest to highlight some of the generic characteristics of any vehicle designed to fly at 100,000 ft that also has range and payload requirements.

For the atmospheric sampling instrumentation (payload) to work, subsonic flight must be maintained (Chambers, 1989). Thus, a limit speed of Mach 0.70 was chosen for the vehicle. This speed makes it convenient to use an unswept wing and simplifies propeller design. The maximum wing loadings are driven into the 6- to 8-lb/ft$^2$ range (fig. 2), while the maximum usable lift coefficients are generally within ±0.2 of 1.0. Although it is possible to design for lower lift coefficients, such designing drives up vehicle size and drives down cruise speed. Lowering cruise speed usually lowers range, especially when considering upper atmosphere winds (fig. 3) or limits to endurance. Thus, it is prudent to design for cruise at a high lift coefficient. Also, the lift coefficient for cruise must be slightly lower (approximately 0.2) than maximum lift (stall) to allow for both gentle maneuvers and gusts.

For a vehicle the size of the stratoplane design, the mean-chord Reynolds number at 100,000 ft is near 600,000. As shown later in the report, a good airfoil at this Reynolds number at Mach 0.65 will have a maximum lift coefficient in the 1.2 to 1.3 range. Thus, the usable lift coefficient for cruise will be near 1.0. At the low Mach number and low-altitude flight condition, the available maximum lift coefficient will be in the 1.8 to 1.9 range. As a point of reference, Mach 0.65 at 100,000 ft corresponds to a dynamic pressure of only 6.9 lb/ft$^2$, a calibrated airspeed of 47 knots, and a true airspeed of 382 knots.

The aspect ratio is driven up by the need to fly with low drag at a high-lift coefficient to minimize the horsepower required for cruise at 100,000 ft. For a propeller-driven engine, thrust is proportional to horsepower divided by true velocity. At 100,000 ft, true velocity is approximately eight times its sea level value at the same dynamic pressure, thus requiring at least eight times the horsepower. Vehicle drag increases with both the higher Mach number and the lower Reynolds numbers associated with high-altitude flight and additionally increases the required horsepower. Also, the difficulties of designing an efficient propeller for the high altitudes also increase the required horsepower.

The total propulsion system weight required to fly at 100,000 ft is approximately five times as heavy for the same horsepower as a reciprocating engine designed to operate at sea level. This additional weight further increases the horsepower required for straight and level flight. For a gasoline engine, fuel used and heat generated are approximately proportional to horsepower. Cooling the propulsion system can become a major source of drag and, thus, a requirement for additional horsepower. A low-drag technique must be used to dissipate the engine and turbocharger heat. Conceptually, the cores of the engine and intercooler radiators must be cowled so that the cooling air is slowed before passing through the core. Then the heated air is accelerated before exiting the cowl. Using this technique, only a slight drag penalty is incurred to cool the engine and intercoolers. An early application of this low-drag cooling technique was incorporated into the F-51 World War II fighter.

The vehicle structure envisioned for this study is primarily all carbon fiber sandwich with a nomex honeycomb core. To meet mission goals, the wing structural weight must be near 1.2 lb/ft$^2$ of wing area, which is approximately the same as the Voyager (Norris, 1988) and Condor (Henderson, 1990) aircraft. This factor is significant as these aircraft have been flown with higher aspect ratios than the proposed stratoplane. Although care must be taken to minimize structural weight, this class of lightweight structure has been achieved using current technology. The fuselage and tail surfaces must be designed in a similar lightweight manner.

2

It is envisioned that the cockpit will be designed for a pressure-suited pilot, but will provide pressurization to the 35,000-ft level as an emergency backup to the pressure suit. The pilot and his equipment are estimated to add 500 lb to the vehicle weight. The main landing gear is located close to the center of gravity and the nosewheel would be steerable.

# DESCRIPTION

The stratoplane (fig. 1) is a conceptual design of a large, manned, single-engine monoplane designed to conduct atmospheric sampling and to validate its engine technology. The vehicle was designed with a gross weight of 11,100 lb and a wing span of 180 ft that gave an aspect ratio of 20.9. The 30-ft-diameter propeller is two-bladed and was clutched into the horizontal position during either a towed takeoff or a power-off landing.

The wings have payload pods 30 ft out on each wing. A box spar and D-tube leading edge are the primary structure of the wing. The inboard box spar contains 4000 lb of fuel. The baseline airfoils are those used for the "Ames wing" in Kennelly et al., 1990. The airfoils are of supercritical profile with a Mach number design of 0.70 and have good low Reynolds number characteristics. The wing thickness varies from 14 percent at the root to 12 percent at the tip.

The horizontal tail shown is a T-tail with capability to deflect through large angles to give good deep-stall capability. The conventional tail location was also investigated and is still viable should deep-stalled flight not be needed. The vertical tail shown is the original tail design that was used for the initial simulation. A vertical tail scaled up by 50 percent in area was later investigated and became the baseline tail for this study.

The identified engine is a gasoline-powered, aluminum-block, liquid-cooled V-8 Thunder aircraft engine (*Jane's*, 1984) that was derated to 600 hp and fitted with a two-speed, clutched gearbox. Level cruise at 100,000 ft and maximum gross weight required most of the 600 hp. The engine radiator is contained in a large pod in the aft fuselage. A three-stage turbocharger system is used with each four-cylinder side of the engine. Intercoolers are located under each inboard wing. The total weight for the engine, turbomachinery, and cooling system is approximately 2200 lb.

# AERODYNAMIC MODEL

The approach taken to generate the aerodynamic model was to first compute the low angle-of-attack data using both the asymmetric vortex lattice program (Lamar and Gloss, 1975) and handbook methods (U.S. Air Force, 1978; Etkin, 1967). Effects of low Reynolds number were included in the determination of maximum lift and profile drag. Data at high angles of attack were estimated using a combination of handbook techniques and the flight results and wind tunnel trends in Sim, 1990. The high angle-of-attack data were included to investigate the deep-stall maneuver as a way of rapidly and safely descending from high altitudes.

The resulting aerodynamic model ranged from an angle of attack of −6° to 90° and from Mach 0 to 0.70. The angle of attack was digitized every 2° from −6° to 20° and every 10° from 20° to 90°. Data were generated for Mach 0, 0.40, 0.60, and 0.70. Moment data in the aero model are referenced to the quarter chord of the mean aerodynamic chord.

## Coefficients

### Lift

Although specific airfoils (Kennelly et al., 1990) have been identified for the stratoplane, data for these airfoils are not available over a wide Mach and Reynolds number range. Thus, data from these airfoils were combined with data

from other sources (McCroskey, 1987; McGhee, Beasley, and Whitcomb, 1979; Althaus, 1980; and Miley, 1982) and used to generate a plot of trends in maximum lift coefficient as a function of Mach and Reynolds number (fig. 4). This same plot is shown with lines of maximum and minimum speed for the stratoplane superimposed on it (fig. 5). Note that there is only a small Reynolds number variation for any given Mach number within the envelope bounded by the speed lines. This allowed the maximum lift coefficient to be modeled as a function of Mach number in the simulation with the Reynolds number effects implicitly included in the Mach number data. Also, the stratoplane flight envelope is well above the subcritical Reynolds numbers (generally below 200,000) where strong viscous effects dominate the flow.

The lift coefficient (fig. 6) was a result of several steps. First, a representative value for the angle of attack at zero lift was chosen based on airfoil camber and trends of similar configurations. Next, the asymmetric vortex lattice program was used to calculate a value for the lift curve slope (at low angles of attack) based only on the planar planform. Then, a hand fairing was drawn between the lift curve slope and the maximum lift coefficient. Finally, a hand fairing was used between the maximum lift coefficient and the data estimated for high angles of attack. The angle of attack corresponding to maximum lift coefficient (for each Mach number) was used as the division between the low angle-of-attack calculations from the asymmetric vortex lattice program and the higher angle-of-attack estimates for the remaining coefficients and derivatives.

## Drag

For the low angles of attack, the estimation of total drag coefficient was separated into the profile and induced components. A generic plot of airfoil profile drag as a function of Reynolds number (fig. 7) was generated from many sources in a manner similar to figure 4. Using the relationship between Reynolds and Mach numbers from figure 5, the data from fig. 7 were used to generate increments in profile drag with Mach number. These increments were then added to an estimated baseline profile drag value of 0.0181. Note that the stratoplane operates in a Reynolds number range that avoids the large profile drag penalties that occur with Reynolds numbers less than 200,000. The induced drag per unit lift-coefficient squared was calculated using the asymmetric vortex lattice program for each Mach number. The profile and the induced terms were then combined to obtain total drag as a function of lift coefficient. Using the lift coefficient data in figure 6, the data were arranged as a function of angle of attack and faired into the high angle-of-attack estimates to give the final drag data in figure 8.

The lift-to-drag ratio was computed using the data in figures 6 and 8 and showed a maximum value of 29 (fig. 9). Because a clean sailplane of similar aspect ratio is expected to have a maximum value near 36, the stratoplane value of 29 was judged reasonable considering the payload pods and the need to provide cooling. The lift and drag coefficients were translated to normal force coefficient (fig. 10) and axial force coefficient (fig. 11) for the simulation model.

## Pitching moment

The slope of the pitching moment coefficient per unit normal force coefficient (static stability parameter) was computed using the asymmetric vortex lattice program and gave a neutral point of approximately 48 percent of the mean chord at low angles of attack. For the high angles of attack, it was judged that the neutral point would move back to approximately 60 percent of the mean chord. This shift in neutral point was included in the static stability parameter for the high angle-of-attack estimates. A representative value for the pitching moment at zero lift was chosen to give a trim value near a lift coefficient of 0.5. An airplane designer can vary this value through choice of airfoil camber, wing incidence, wing twist, and tail incidence. The pitching moment coefficients (fig. 12) were computed by multiplying the static stability parameter by the normal force coefficient from figure 10.

4

## Derivatives

### Elevator and stabilizer control effectiveness

The primary longitudinal control was defined as the elevator. Trim and transition to and from deep-stalled flight was accomplished using the stabilizer which, on the simulator, was controlled using a separate side lever. In deep stall, the stabilizer is somewhat aligned with the free-stream air (with attached flow) allowing both control surfaces to maintain reasonable control effectiveness. The low angle-of-attack values for pitching moment coefficient and normal force coefficient derivatives were computed using the asymmetric vortex lattice program. Again, these values were faired into the high angle-of-attack estimates. Trends in the axial force derivatives were taken primarily from the high angle-of-attack estimates. The resulting derivatives are presented in figures 13(a), (b), and (c) for the elevator and figures 14(a), (b), and (c) for the stabilizer.

### Longitudinal damping

The damping in pitching moment coefficient due to pitch rate (fig. 15(a)) and the normal force coefficient due to pitch rate (fig. 15(b)) were both calculated using the asymmetric vortex lattice program. Because these damping terms primarily result from the stabilizer and because the stabilizer maintains attached flow at high angles of attack (in deep stall), the damping derivatives were held constant over angle of attack.

### Sideslip

The low angle-of-attack values for yawing moment coefficient and side force coefficient due to sideslip derivatives were calculated using the asymmetric vortex lattice program with a side view planform panel model and the original small vertical tail. Data for high angles of attack were taken from the high angle-of-attack estimates. The yawing moment coefficient due to sideslip derivative (fig. 16) represents the directional stability and is lower than normally desired for an unaugmented vehicle. The side force due to sideslip derivative is presented in figure 17. The baseline vertical tail, with 50 percent more area (large tail), was modeled using the multiplication factors from table 1. These factors were obtained using the ratio of the asymmetric vortex lattice program calculations of panel models with the two tail sizes.

Table 1. Vertical tail-size multipliers.*

| Derivative | Multiplier |
|---|---|
| Change in side force coefficient due to angle of sideslip | 1.31 |
| Change in yawing moment coefficient due to angle of sideslip | 1.43 |
| Increment in rolling moment coefficient due to rudder | 2.23 |
| Increment in side force coefficient due to rudder | 1.89 |
| Increment in yawing moment coefficient due to rudder | 1.82 |
| Yaw damping due to yaw rate parameter | 1.50 |

*Used to convert from original tail to 50 percent larger tail area.

The rolling moment coefficient due to sideslip is commonly called the effective dihedral derivative because it is strongly influenced by wing dihedral. Although elastic bending properties of the wing are not yet well defined, the lightweight structure of the stratoplane will give considerable wing dihedral. For this study, a curvalinear dihedral with a 10° tangent line at the wingtip was used. Handbook calculations (U.S. Air Force, 1978) show that a rigid wing with this dihedral will produce the low angle-of-attack values shown in figure 18(a). The high angle-of-attack values were from the high angle-of-attack estimates. However, aeroelastic relief in sailplanes is known to alleviate the effective dihedral. Considering the scope of this study and the indeterminate aeroelastics, it was decided to bound the effective dihedral estimate from 25 percent of this value to the full value. Both values were studied in the simulation, with the baseline value the 25 percent value (fig. 18(b)).

### Aileron

The rolling moment coefficient due to aileron is the primary roll control derivative (fig. 19(a)). The derivative was obtained using the asymmetric vortex lattice program calculations for low angles of attack and was combined with the high angle-of-attack estimates. The yawing moment coefficient (fig. 19(b)) and corresponding sideforce coefficient due to aileron (fig. 19(c)) were estimated based on the premise that a differential control scheme (more up than down aileron) would be implemented. Thus, proverse yaw was attained at low angles of attack similar to the data in Sim, 1990.

### Rudder

Rolling moment coefficient due to rudder (fig. 20(a)), yawing moment coefficient due to rudder (fig. 20(b)), and sideforce coefficient due to rudder (fig. 20(c)) were calculated using the asymmetric vortex lattice program for low angles of attack and combined with the high angle-of-attack estimates. The 50-percent larger rudder that accompanied the large, vertical tail was modeled in the simulation using the multiplication factors from table 1.

### Lateral-Directional Damping

The change in rolling moment coefficient due to roll rate parameter, the primary roll damping derivative (fig. 21(a)), was calculated at low angles of attack using the asymmetric vortex lattice program and combined with the high angle-of-attack estimates. The change in yawing moment coefficient due to roll rate parameter (fig. 21(b)) and the change in rolling moment coefficient due to yaw rate parameter (fig. 21(c)) were both estimated based on the trends of Sim, 1990. The change in yawing moment coefficient due to yaw rate parameter (fig. 21(d)), the primary damping in yaw derivative, was derived using the general levels from the asymmetric vortex lattice program and the data in U.S. Air Force, 1978. The increase in yaw damping due to the large vertical tail was modeled in the simulation using the multiplication factors from table 1.

## Lateral-Directional Trim

A bias term in the rolling moment, yawing moment, and sideforce coefficients were included to model the poststall. While stall is often treated as a symmetric maneuver, it rarely happens that way. Conditions such as rigging, uncoordinated flight, and turn rate will cause one wing to stall first while the other wing remains attached. This effect is accentuated by long wingspans. Once the second wing also stalls, a greater degree of symmetry is retained.

For the Schweizer SGS 1-36 sailplane in Sim, 1990, the trim biases were of greater magnitude than the available control power during the poststall region. The values shown for the plots of rolling moment coefficient bias (fig. 22),

yawing moment coefficient bias (fig. 23), and side force coefficient bias (fig. 24) were multiplied by scale factors within the simulation of typically ±10.

# MASS AND PROPULSION MODELS

## Mass Model

For the mass properties, a weight and a primitive shape were assigned to 31 vehicle components. The vehicle was defined as symmetric in planform. The moments of inertia and mass centroid locations were then generated using a spreadsheet and are summarized in table 2. For the simulation, the longitudinal center of gravity was at 39 percent of the mean chord, while the neutral point was near 48 percent. The high vertical center of gravity is a result of the wing dihedral. Much of the simulation study was conducted using a 2000-lb middle fuel weight, while the full and empty conditions were given limited study.

Table 2. Mass properties.

| Fuel weight, lb | 0 | 2,000 | 4,000 |
|---|---|---|---|
| Total vehicle weight, lb | 7,100 | 9,100 | 11,100 |
| Rolling moment of inertia, slug-ft$^2$ | 132,200 | 136,900 | 141,600 |
| Pitching moment of inertia, slug-ft$^2$ | 36,840 | 36,990 | 37,150 |
| Yawing moment of inertia, slug-ft$^2$ | 162,500 | 167,300 | 172,000 |
| Roll-to-yaw cross product of inertia, slug-ft$^2$ | 4,620 | 4,680 | 4,740 |
| Center of gravity behind quarter chord reference, ft | 1.32 | 1.32 | 1.32 |
| Center of gravity above thrust centerline reference, ft | 1.13 | 1.03 | 0.97 |

## Propulsion Model

The propulsion model included fuel flow, propeller efficiency, and propeller inertial effects. The throttle lever and fuel flow was proportional to hp. The pilot could select either 250 rpm for low-altitude flight or 500 rpm for high-altitude flight. The propeller efficiency (fig. 25) was calculated using the Hamilton-Standard data in Lan and Roskam, 1980. An integrated propeller lift coefficient of 0.15 was chosen to minimize Mach number effects. The 500-rpm line is questionable at altitudes lower than 40,000 ft as a result of the very flat pitch needed at these altitudes. Use of an intermediate propeller speed of approximately 375 rpm would benefit climb performance in the middle altitudes. However, this speed was not considered significant for the simulation. The propulsion model used was considered to be the minimum needed for a stability and control simulation.

# SIMULATION RESULTS

## Approach

Both low- and high-altitude nominal flight conditions (table 3) were chosen for evaluation. Flying qualities of the unaugmented vehicle were first evaluated to find out whether the vehicle could be flown without a control system. The maneuvers investigated included climb, descent, 20° bank turns, and recovery from control perturbations.

7

Table 3. Nominal flight conditions studied.

| Reference name | Low altitude | High altitude |
|---|---|---|
| Altitude, ft | 10,000 | 100,000 |
| Angle of attack, deg | 5 | 3 |
| Dynamic pressure, lb/ft$^2$ | 6.4 | 6.4 |
| Fuel weight, lb | 2,000 | 2,000 |
| Mach number | 0.08 | 0.63 |
| Reynolds number, per ft | 4,240,000 | 66,900 |
| True velocity, knots | 50.6 | 367 |

Early investigations on the simulator showed the vehicle to be difficult to fly at any altitude as a result of near-neutral dutch roll oscillations. Thus, a vertical tail with 50 percent more area (large tail) was investigated and became the baseline configuration for this simulation study. With the large tail, the vehicle could be flown without control augmentation, but still exhibited very lightly damped dutch roll characteristics.

Linear analyses were conducted to provide insight into the dynamic modes of the vehicle and to substantiate the control system design. The linear analysis results are displayed in classic root locus plots. The scope of the control system evaluation was limited to primarily the basic feedback of rates and attitudes. Safe and rapid descending either from 100,000 ft or through the turbulent middle altitudes was investigated by intentionally deep stalling the stratoplane.

## Unaugmented Simulator

At low altitudes, the vehicle showed good longitudinal short-period stability, but the phugoid mode was near neutrally stable (fig. 26). High aspect ratio causes a decrease in phugoid damping and an increase in phugoid frequency. Although the phugoid can be damped by the pilot, it does increase pilot workload as a result of the difficulty to attain and hold longitudinal trim. Neither airspeed nor rate of climb could be precisely controlled.

At low altitudes, the vehicle showed good roll stability; however, the dutch roll mode was lightly damped and the spiral mode was slightly unstable (figs. 27 and 28). The spiral mode can be damped by the pilot but requires some attention. The loose dutch roll mode comes from generally low directional stability as a result of both a large fuselage side area and a minimal-sized vertical tail. The larger tail improved the overall lateral-directional flying qualities but still did not produce a good flying vehicle. The vehicle was difficult to fly and required constant pilot attention.

The stratoplane tended to fly at indicated airspeeds near 45 knots, which at low altitude is near 45 knots true. With these low airspeeds and a loose dutch roll, the pilot must be careful to avoid excessive sideslip. With the small tail, this task was difficult in the presence of larger dutch roll oscillations. Using the higher values of the effective dihedral derivative in fig. 18(a) made the vehicle more difficult to control as a result of the increased tendency for the pilot to couple into the sideslip excursions.

At 100,000 ft, the true velocity is approximately eight times greater than at sea level for the same indicated velocity. Because the aerodynamic damping and force terms are divided by true velocity, they are significantly decreased at high altitudes. The reduction in longitudinal damping results in a neutrally stable phugoid mode (fig. 29). This results in a vehicle that can be safely damped but cannot be flown with precision because of the inability to stabilize rate of climb. With full fuel, the flying tasks were more difficult as a result of the small margin between cruise lift and stall.

At a 100,000-ft altitude, the reduction in lateral-directional damping produced an unstable spiral and a barely stable dutch roll mode that dominated the vehicle response (fig. 30). With the larger vertical tail, it was still possible to manually fly the unaugmented vehicle, but only with high pilot workload. Piloting the airplane required constant

8

attention. Fortunately, the side force terms are also divided by true velocity, alleviating the tendency to generate excessive sideslip. Unaugmented flight with the original small vertical tail was still possible, but only with very high pilot workload. With either vertical tail, the effects of using higher values of the effective dihedral derivative in figure 18(a) were masked by the difficulty of maintaining control of the vehicle.

## Augmented Simulator

The goal of the control system development task was to investigate the value of a relatively uncomplicated low-gain system. Thus, with an exception, only gains were used in the feedback loops, and forward-loop compensation was not used. A low set of gains was desired to minimize actuator rate and power requirements. As a result of the ease of mechanization, the feedbacks were tried first on the simulation and then later analyzed using linear analysis. The analysis results validated the control system design and cross-checked the simulation. Much of the understanding of how the feedbacks affects particular modes comes from the linear analysis; however, the resulting flying qualities come from the simulation.

In the longitudinal axis, the goal was to stabilize the phugoid at high altitudes and, preferably, eliminate its second-order response. The goal was accomplished by feeding back flightpath angle to the elevator (fig. 31). At low gains in the range of 0.2 to 0.3, the phugoid was stabilized, but with an underdamped response that resulted in a minor tendency to search for trim. With gains of approximately 0.6, the phugoid became overdamped and produced a good flying vehicle with little overshoot. At higher gains of approximately 0.8 and 0.9, the phugoid eigenvalues were driven real, also producing a good flying vehicle with no tendency to overshoot.

However, the high flightpath feedback gains reduced the short-period damping. As a countermeasure, pitch rate feedback was fed to the elevator (fig. 32), adding damping to the short period without significantly affecting the phugoid. The resulting control system (fig. 33) provides good longitudinal flying qualities at all altitudes with the same set of fixed gains. A minor degradation in flying qualities can be traded for lower gains.

The approach taken for the lateral-directional control system was to feedback the states (angles of bank and sideslip, and roll and yaw rate) to the appropriate control (aileron or rudder). Positive spiral stability was achieved by feeding the bank angle to the aileron to obtain a simple wings leveler. At low altitude this required a gain in the 0.3 to 0.4 range (fig. 34(a)), while at a high altitude only a gain between 0.04 and 0.1 sufficiently stabilized the spiral (fig. 34(b)). Higher gains at high altitude would drive the spiral too stable, destabilize the roll mode, and destabilize the dutch roll mode. The roll rate was fed to the aileron (fig. 35) to increase roll damping and slightly improve flying qualities. A roll rate gain of 0.3 was used at both high and low altitudes.

Also, yaw rate, with a washout filter, was fed to the rudder (fig. 36) to improve yaw damping. The yaw rate feedback with a gain of 0.1 slightly improved the flying qualities. However, with other loops closed (not shown), higher yaw rate gains degraded the flying qualities and made yaw rate an ineffective feedback. The unity time constant chosen for the yaw rate washout filter is perhaps too large, but was not refined as a result of the ineffectual nature of the yaw rate feedback.

The use of bank angle and the rates (fig. 37) greatly improved the lateral-directional flying qualities and produced a safe flying vehicle at all altitudes with either the original or the larger vertical tail. However, the small sideslip oscillations resulting from a loose dutch roll mode were not totally eliminated. Feeding back angle of sideslip to the rudder (fig. 38(a)) was studied but did not produce significant improvement until unreasonably high gains greater than 1 were used. Note that the angle of sideslip feedback loop was presented with the other loops closed as a result of strong coupling with the bank angle feedback loop.

Variations in the effective dihedral derivative from the 25-percent baseline value (fig. 18(b)) to the 100-percent value (fig. 18(a)) produced interesting results. At low altitudes, the higher values of the effective dihedral derivative provided more dutch roll stability and gave slightly better handling qualities. At high altitudes with the baseline 25 percent value, the dutch roll was near neutral stability and oscillated primarily in the yaw axis. With the full

9

baseline values of effective dihedral, the handling qualities were degraded as a result of additional rolling motion in the dutch roll mode.

One unconventional lateral-directional feedback was studied and found to provide benefits for specific situations. For high altitudes, angle of sideslip, with the wrong sign on the gain, was often feedback to the aileron (fig. 38(b)). Better flying qualities were produced, especially when high values of the effective dihedral parameter were modeled. The gain used was −0.1, as higher negative gains drove the dutch roll mode down in frequency and produced instability. Good lateral-directional flying qualities require a more complete study.

## Rapid Descent

In an emergency, the pilot may need to rapidly descend to altitudes below 48,000 ft where a pressurized environment is not required. Although an escape capsule is viable, it has the undesirable side effect of losing the vehicle. Two ways of rapidly descending are with either a controlled deep-stall maneuver or with a large external drag device like a parachute to limit maximum airspeeds. Although a large external drag device is feasible, it was decided to direct the simulation study toward the deep-stall maneuver that uses stalled wings for its drag device.

The deep-stall maneuver has been used throughout aviation history and has been shown to be safe and repeatable (Sim, 1990). The deep-stall maneuver can be divided into three stages: entry to very high angles of attack, stabilized flight at very high angles of attack (typically 40° to 70°), and recovery back to low angles of attack. To control deep stall, the stabilizer needs to deflect through large angles. Thus, the airflow over the horizontal tail can remain attached while the wing is fully stalled. The stabilized angle of attack is then a function of stabilizer and elevator angle, with nominal values in the 40° to 60° range. During the simulation studies, the control system was engaged using the high altitude, low angle of attack, and gain set.

A special technique was needed for the entry into deep stall to keep the peak pitch attitudes less than 15° to 20° and to avoid the excessive 50° to 60° values that were easy to attain. With power off, the vehicle was slowed to stall using the elevator. The elevator was first used to slowly raise the angle of attack to approximately 25°. The stabilizer was next slowly moved to further increase the angle of attack while the elevator was relaxed to its neutral position. The pitch attitude then stabilized at −12° and airspeed indicated at approximately 38 knots. The entire transition to a stabilized high angle of attack required approximately 20 sec to complete.

During stabilized high angle-of-attack flight, the pitch and roll axis were relatively steady, but the heading wandered. Active use of the rudder tended to excite the dutch roll mode, which could be easily damped using aileron. For a deep-stall maneuver that stabilized at an angle of attack of 70°, it took 4 min and 20 sec to descend from 100,000 ft to 40,000 ft. Rate of sink peaked at 430 ft/sec at approximately 90,000 ft and decreased to 130 ft/sec at 40,000 ft.

Recovery to low angles of attack also required special flight techniques to limit the required peak airspeed. First, the angle of attack was slowly lowered to approximately 25° using the stabilizer. The elevator was used to rapidly (over approximately 2 sec) push the nose down and thus lower the angle of attack. Then, the nose was slowly pulled back and the horizontal stabilizer neutralized. The indicated airspeeds required for recovery were at least 58 knots for a recovery at 75,000 ft and at least 52 knots for a recovery at 35,000 ft. Unfortunately, the corresponding equivalent airspeeds required for the recovery are slightly higher than needed for any other maneuver studied.

The deep-stall maneuver is viable for this class of vehicle should rapid descent be necessary. However, incorporation of deep-stall capability may require either an increased maximum airspeed limit or a small drag control device to limit peak airspeeds.

10

### Aileron Size

The ailerons were initially sized to be similar to those used on many low-performance sailplanes. However, during the simulation, less than half the total ±25° maximum deflection for each aileron was used. Thus, smaller ailerons would have been adequate.

# CONCLUDING REMARKS

The stratoplane is a conceptual design of a large, manned single-engine monoplane designed to conduct atmospheric sampling and to validate its engine technology. The vehicle was designed with a gross weight of 11,100 lb, a wingspan of 180 ft, and a propeller 30 ft in diameter. To study problems associated with the flight characteristics of such a large, lightweight vehicle, a manned real-time simulation was developed. In support of the simulation, mathematical models of the aerodynamics, mass properties, and propulsion system were developed.

The simulation was initially conducted with the unaugmented vehicle to determine the needs for a control augmentation. The unaugmented longitudinal flying qualities were dominated by a lightly damped phugoid at low altitude and a neutrally stable phugoid at 100,000 ft. The vehicle could be safely flown in the longitudinal axis, but could not be precisely controlled as a result of the difficulty in maintaining trim. In the lateral-directional axis, the flying qualities were dominated by lightly damped dutch roll oscillations. The vehicle required constant pilot attention at the lower altitudes and very high pilot workloads at high altitudes.

Control augmentation was investigated using basic feedbacks. For the longitudinal axis, flightpath angle and pitch rate feedback were sufficient to damp the phugoid mode and produce good flying qualities. In the lateral-directional axis, bank angle, roll rate, and yaw rate feedbacks were sufficient to provide a safe vehicle with acceptable handling qualities.

Intentionally deep stalling the stratoplane was investigated for a safe and rapid descent from either 100,000 ft or through the turbulent middle altitudes. It was concluded that the deep stall maneuver is a viable maneuver for this class of vehicle. However, incorporation of deep-stall capability may require either an increased maximum airspeed limit or a small drag device to limit peak airspeeds.

# REFERENCES

1. Althaus, Dieter, *Profilpolaren für den Modellflug* (Polars of Airfoils for Model Airplanes), Neckar-Verlag, Villengen-Schwenningen, Germany, 1980.

2. Chambers, Alan, and R. Dale Reed, "A Very High Altitude Aircraft for Global Climate Research," *Unmanned Systems*, vol. 8, no. 3, Summer 1990, pp. 14–19.

3. Chambers, Alan B., *Global Stratospheric Change: Requirements for a Very-High-Altitude Aircraft for Atmospheric Research*, NASA CP-10041, 1989.

4. Etkin, Benard, *Dynamics of Flight: Stability and Control*, John Wiley & Sons, New York, London, and Sydney, 1967.

5. Henderson, Breck W., "Boeing Condor Raises UAV Performance Levels," *Aviation Week and Space Technology*, vol. 132, no. 16, April 23, 1990, pp. 36–38.

6. *Jane's All the World's Aircraft 1983–84*, Jane's Publishing Co., New York and London, 1984, p. 843.

7. Kennelly, Robert A., Ilan M. Kroo, James M. Strong, and Ralph L. Carmichael, *Transonic Wind Tunnel Test of a 14% Thick Oblique Wing*, NASA TM-102230, 1990.

8. Lamar, John E., and Blair Gloss, Subsonic Aerodynamic Characteristics of Interacting Lifting Surfaces with Separated Flow Around Sharp Edges Predicted by a Vortex-Lattice Method, NASA TN D-7921, 1975.

9. Lan, C. Edward, and Jan Roskam, *Airplane Aerodynamics and Performance*, Roskam Aviation & Engineering Corp., Ottawa, KN, 1980, pp. 289–329.

10. McCroskey, W.J., *A Critical Assessment of Wind Tunnel Results for the NACA 0012 Airfoil*, NASA TM-100019, 1987.

11. McGhee, Robert J., William D. Beasley, and Richard T. Whitcomb, *NASA Low- and Medium-Speed Airfoil Development*, NASA TM-78709, 1979.

12. Miley, S.J., *A Catalog of Low Reynolds Number Airfoil Data for Wind Turbine Applications*, Texas A&M Univ., College Station, TX, Feb. 1982.

13. Norris, Jack, *Voyager, The World Flight: The Official Log, Flight Analysis and Narrative Explanation*, Jack Norris, Publisher, Northridge, CA, 1988.

14. Sim, Alex G., *Flight Characteristics of a Modified Schweizer SGS 1-36 Sailplane at Low and Very High Angles of Attack*, NASA TP-3022, 1990.

15. Smith, J.P., Lawrence J. Schilling, and Charles A. Wagner, *Simulation at the Dryden Flight Research Facility from 1957 to 1982*, NASA TM-101695, 1989.

16. U.S. Air Force, *USAF Stability and Control DATCOM*, Flight Control Division, Air Force Flight Dynamics Laboratory, Wright-Patterson Air Force Base, OH, April 1978.

Maximum:

| | |
|---|---|
| Altitude | 100,000 ft |
| Range | 3,700 mi |
| Payload | 1,000 lb |
| Fuel | 4,000 lb |
| Gross weight | 11,000 lb |

Vertical tail area = 48.6 ft$^2$

Wing:
Span = 180 ft
Area = 1550 ft$^2$
Aspect ratio = 20.9

Two engine radiators,
4 by 8 ft in aft body

Air-to-air intercoolers for
three-stage supercharger system

Fuel in
box spar

Removable pilot module
unmanned conversion

Two payload pods,
500 lb each

Thunder engine,
600 hp

Two-speed gearbox

Propeller, 30 ft in diameter

Two first-stage 3-ft-diameter turbo-superchargers

910567

(a) Conceptual layout.

Figure 1. Stratoplane.

13
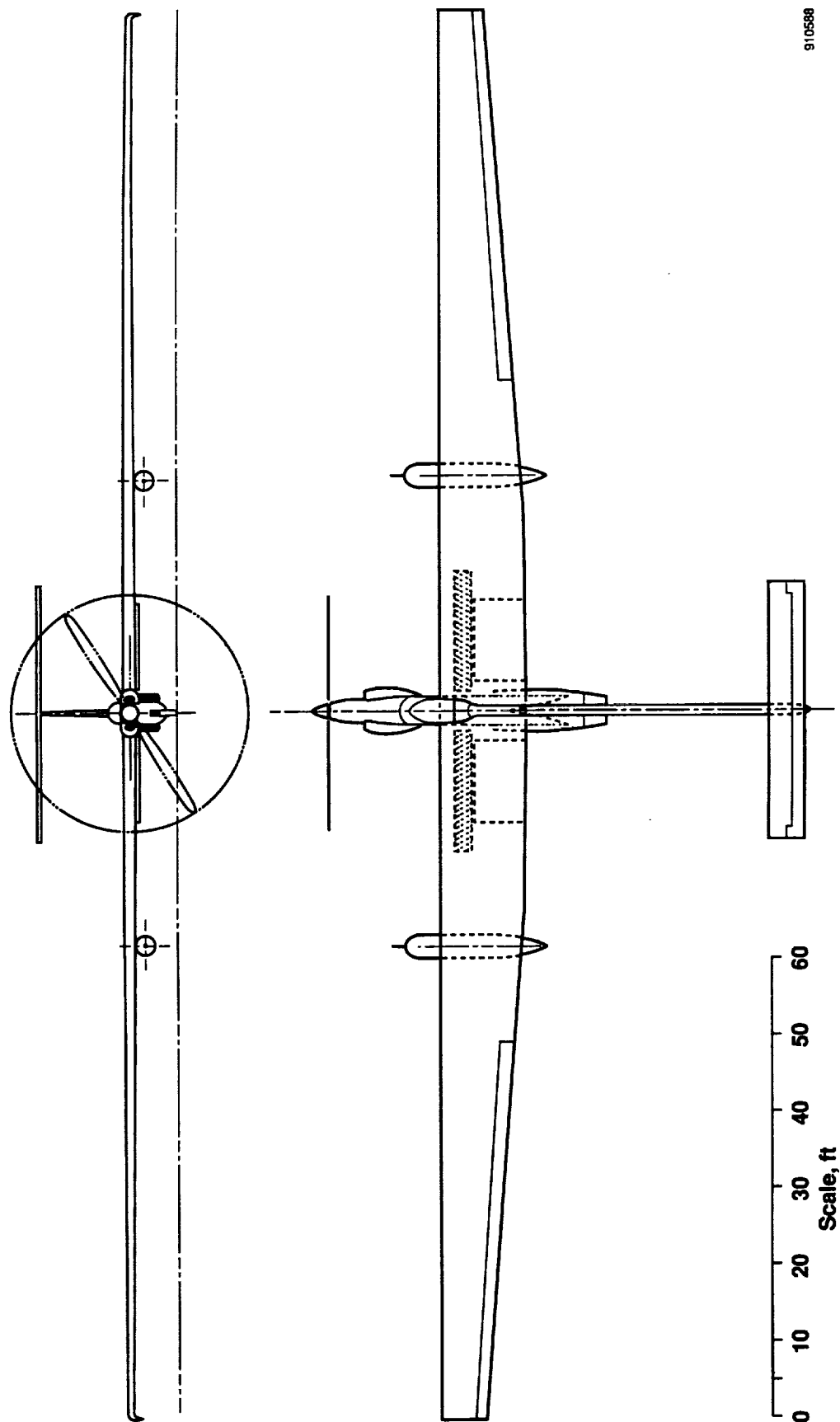
(b) Two-view drawing.

Figure 1. Concluded.

Scale, ft

910588

14
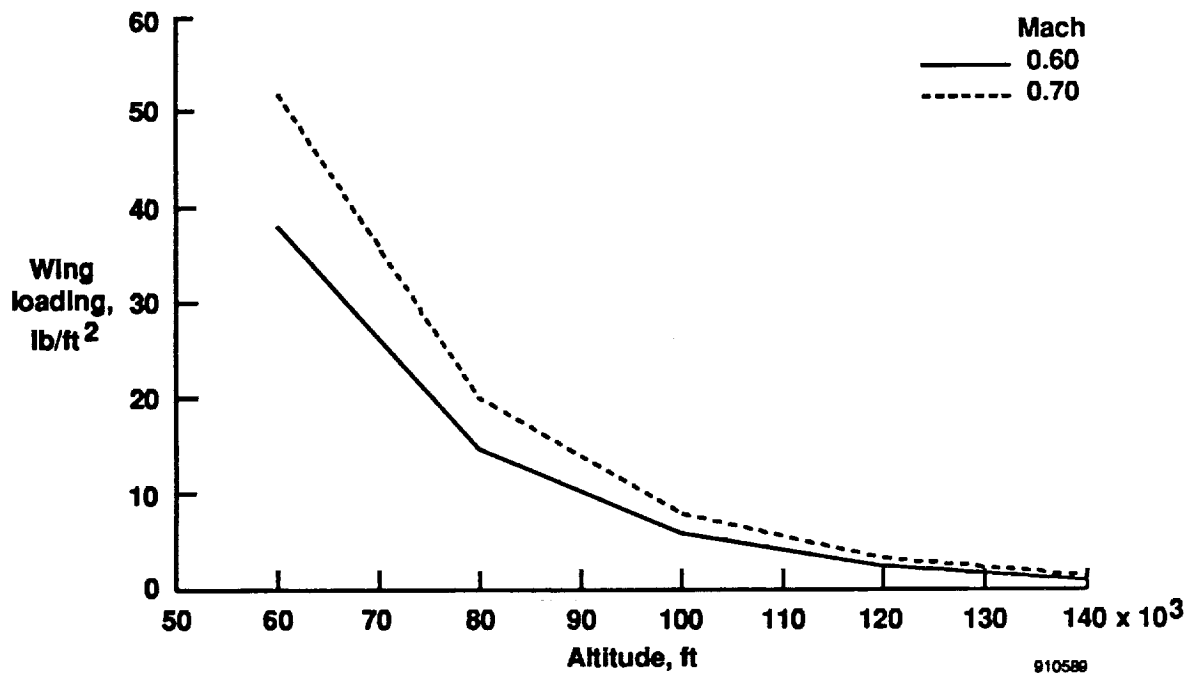
Figure 2. Wing loading at high altitudes with lift coefficient of 1.0.
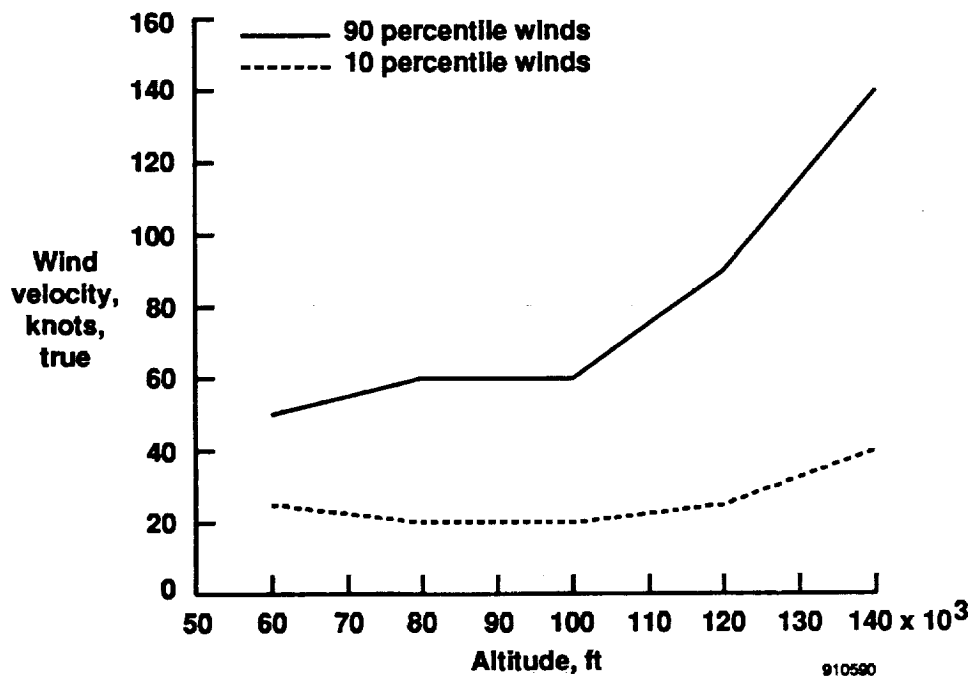


Figure 3. Generic winds at high altitudes.
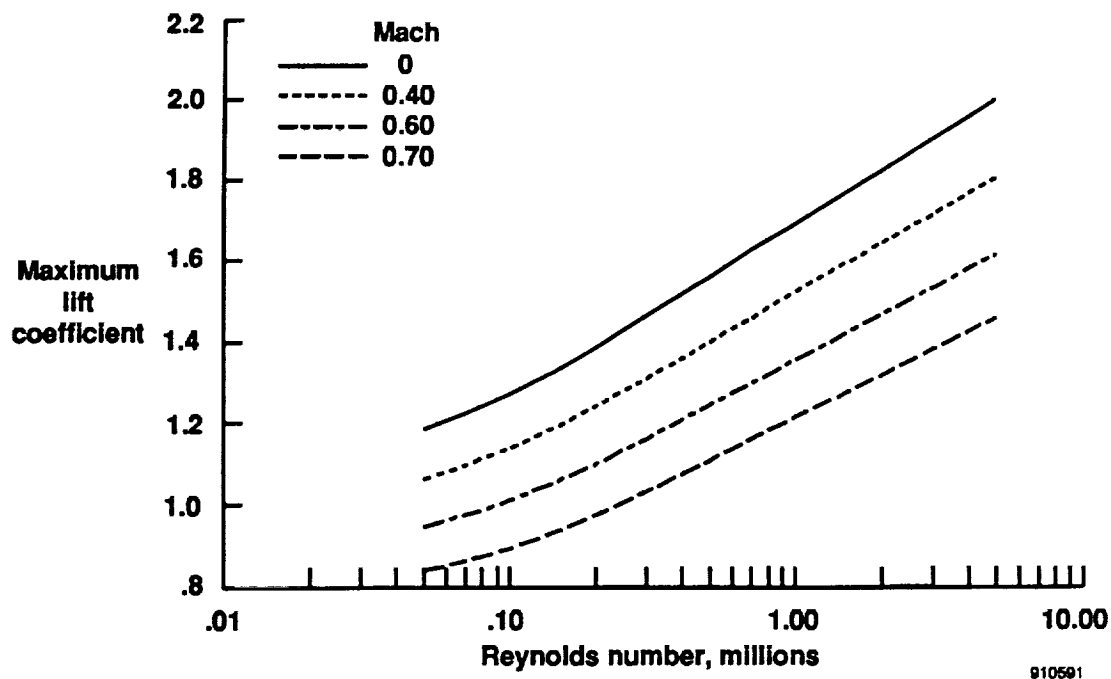
Figure 4. Generic trends in maximum lift coefficient.
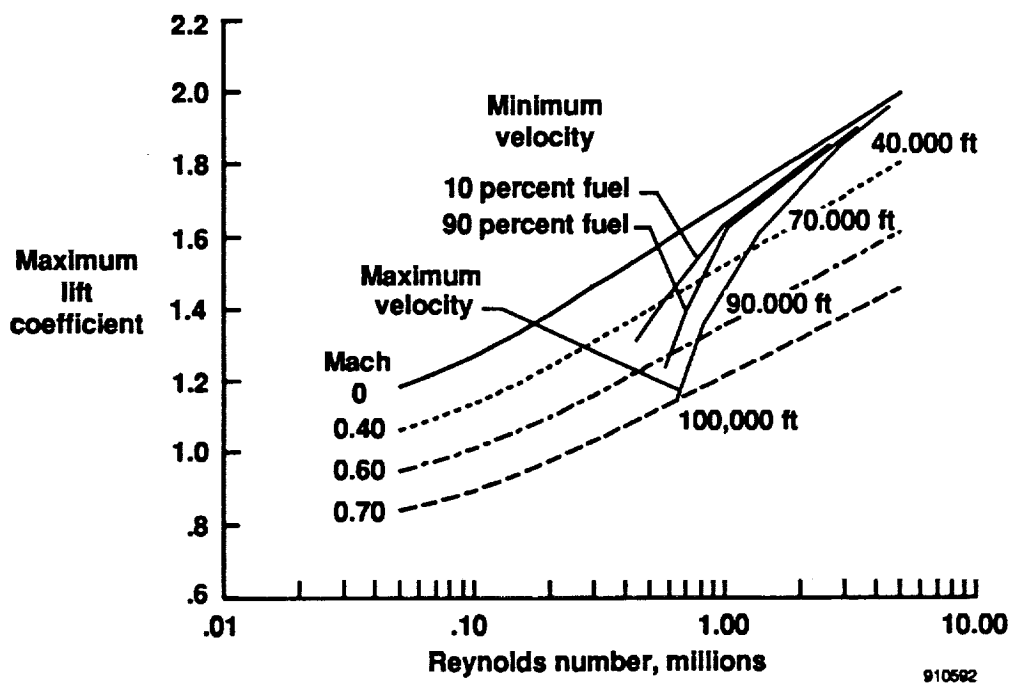


Figure 5. Lines of minimum and maximum velocity for stratoplane superimposed on figure 4; Reynolds number based on mean chord.

16
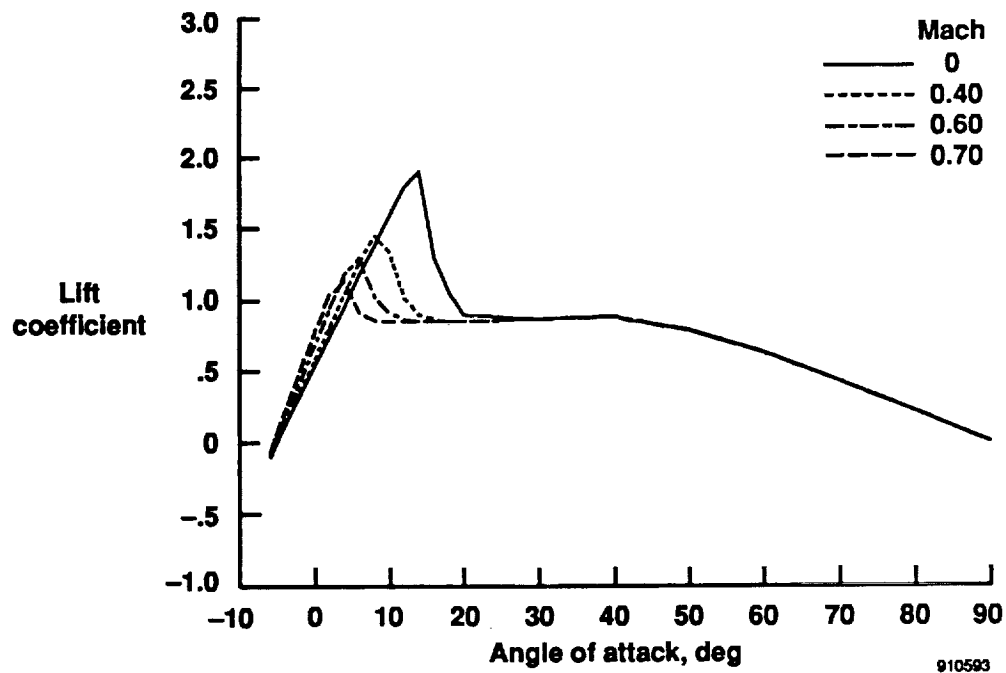
Figure 6. Lift coefficient.
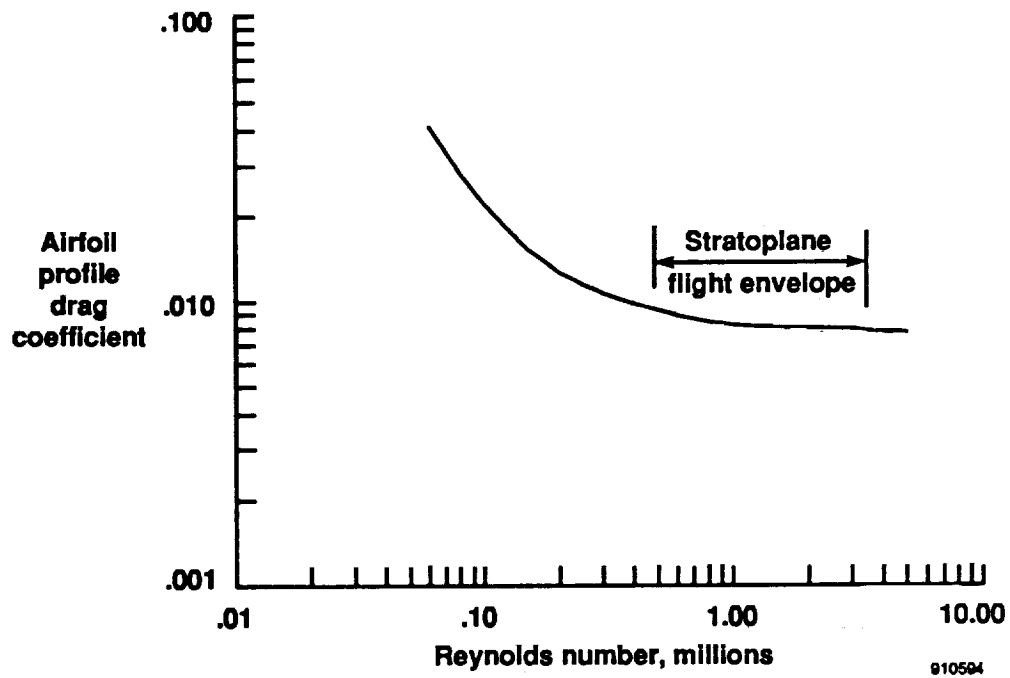


Figure 7. Generic trends in airfoil profile drag coefficient with lift coefficient of 1.0.
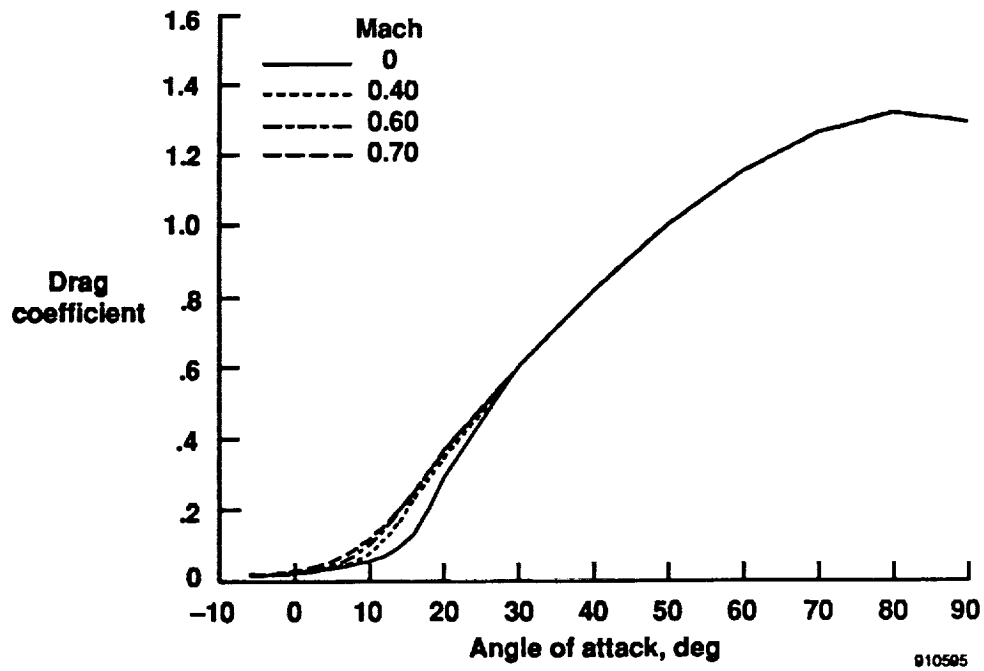
Figure 8. Drag coefficient.
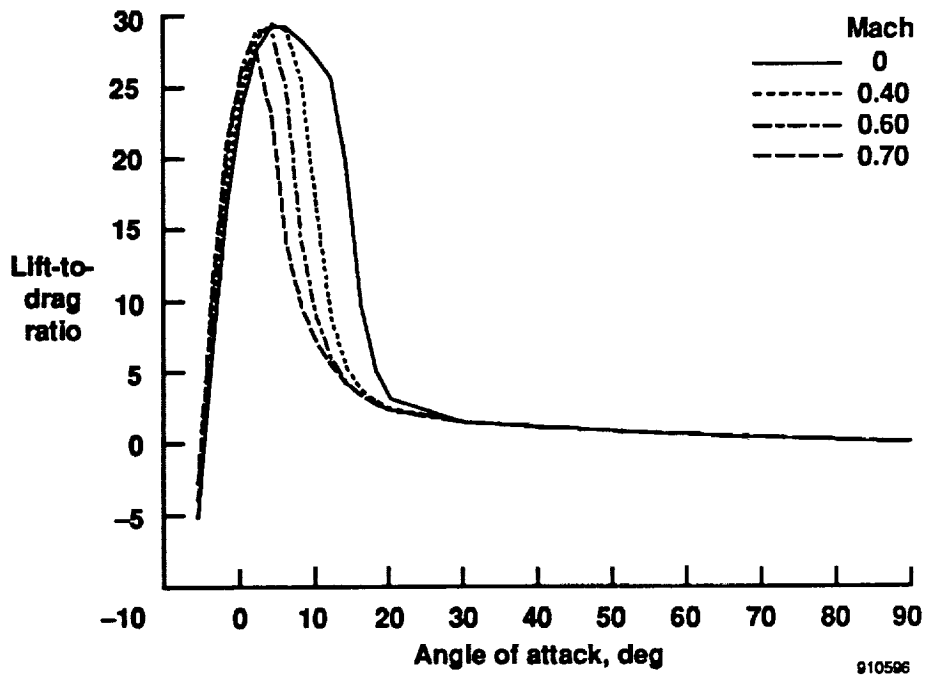


Figure 9. Longitudinal performance efficiency parameter.

18
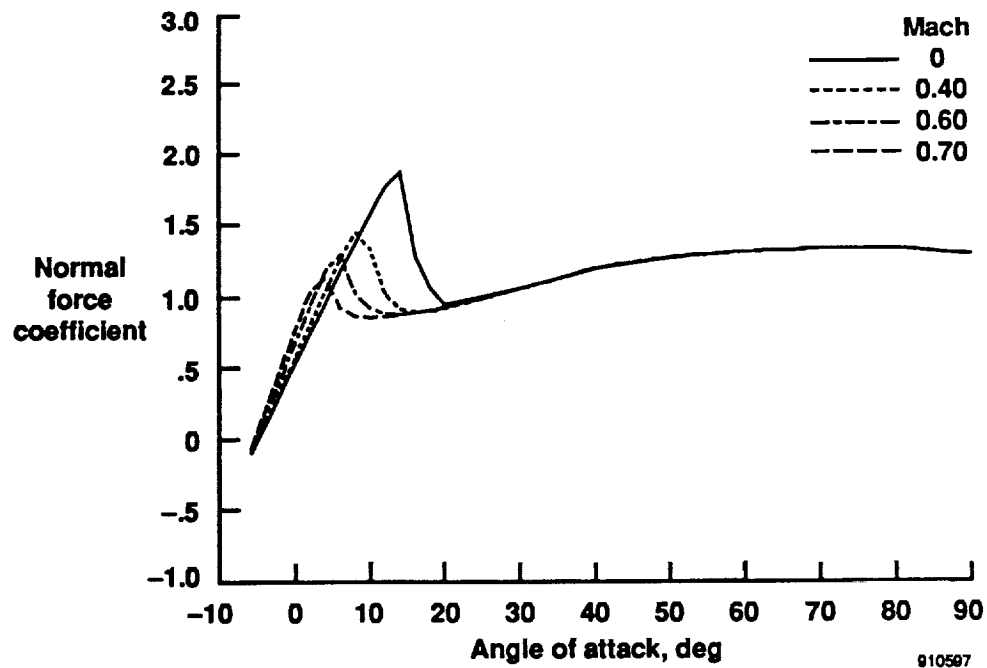
Figure 10. Normal force coefficient.
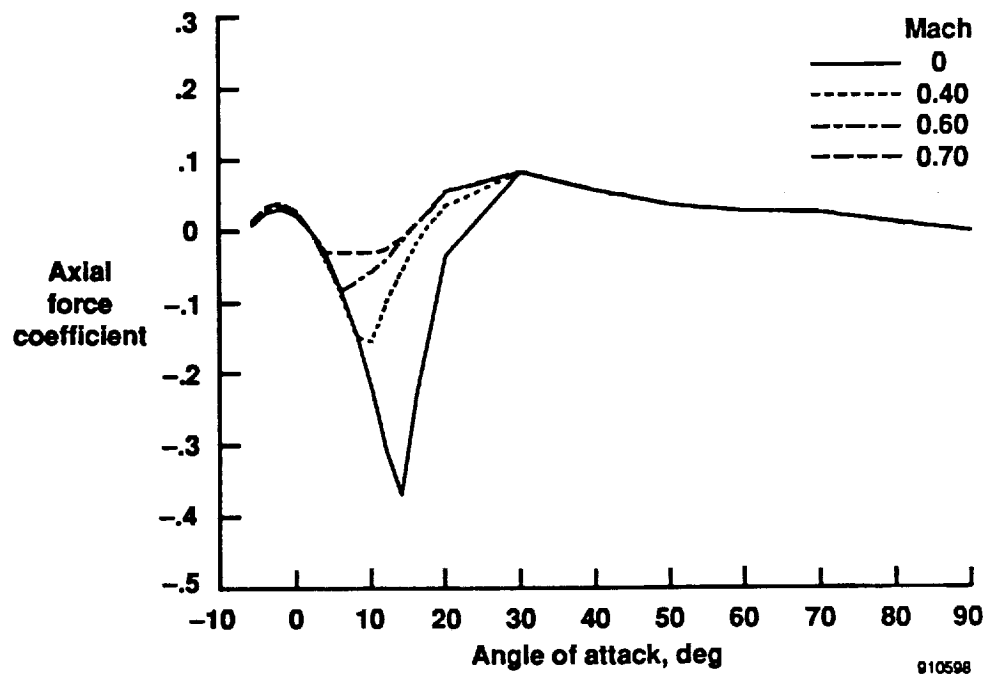


Figure 11. Axial force coefficient.
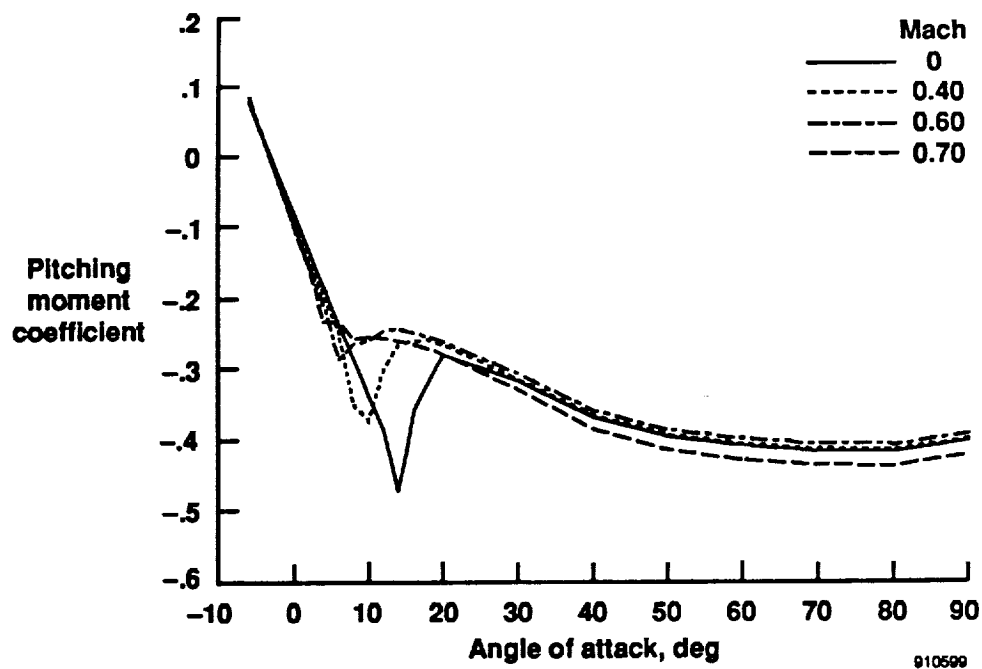
Figure 12. Pitching moment coefficient.
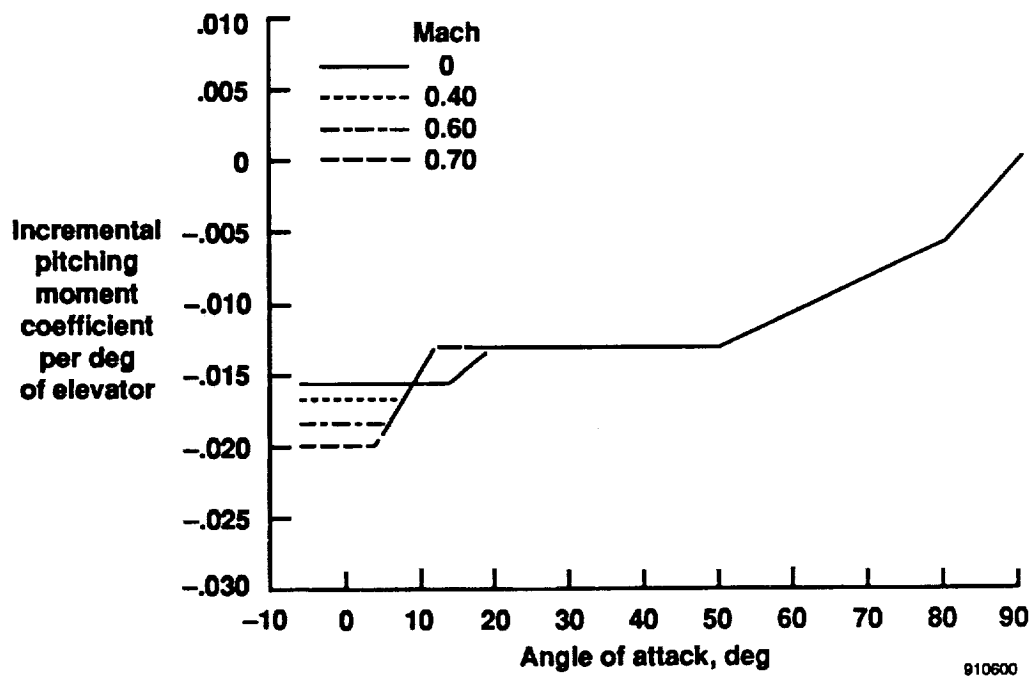


(a) In pitching moment coefficient.

Figure 13. Elevator control effectiveness.

20
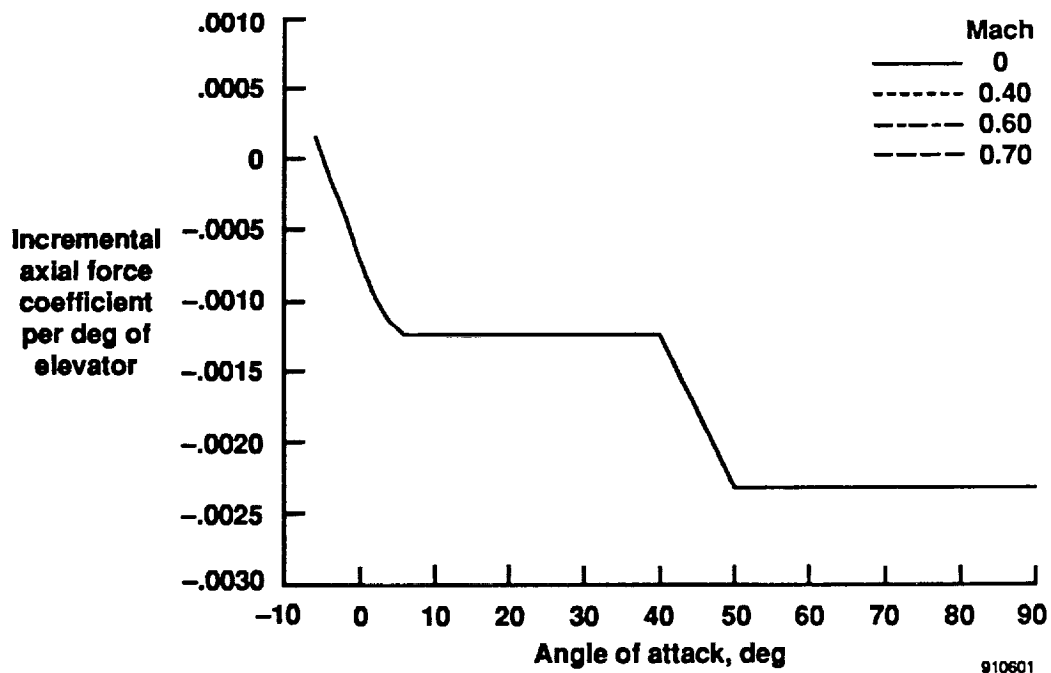
(b) In axial force coefficient.
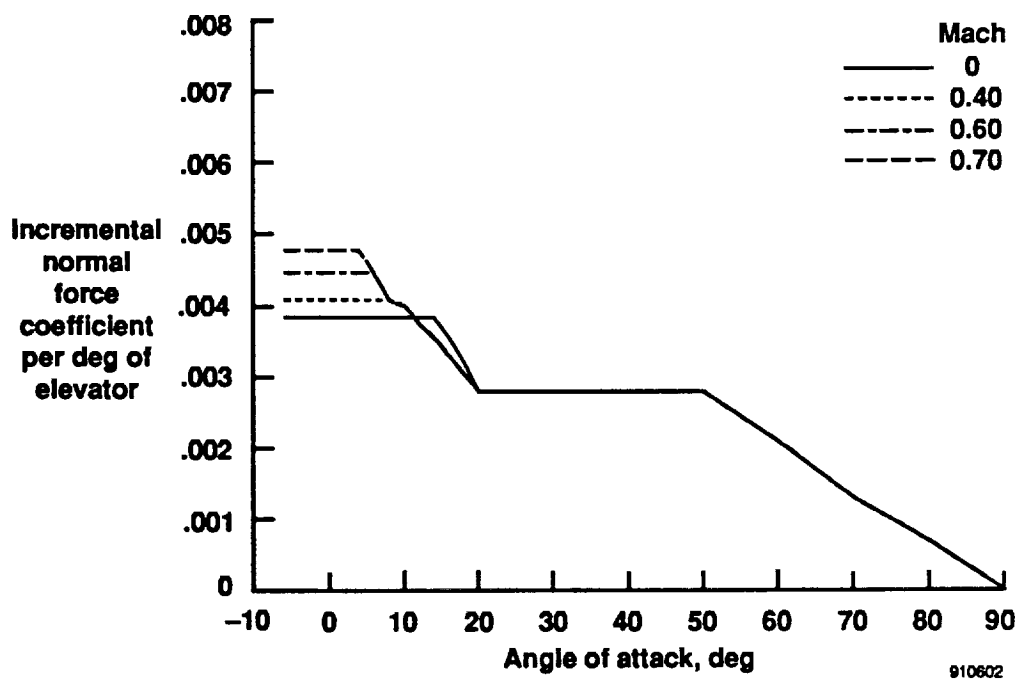


(c) In normal force coefficient.

Figure 13. Concluded.
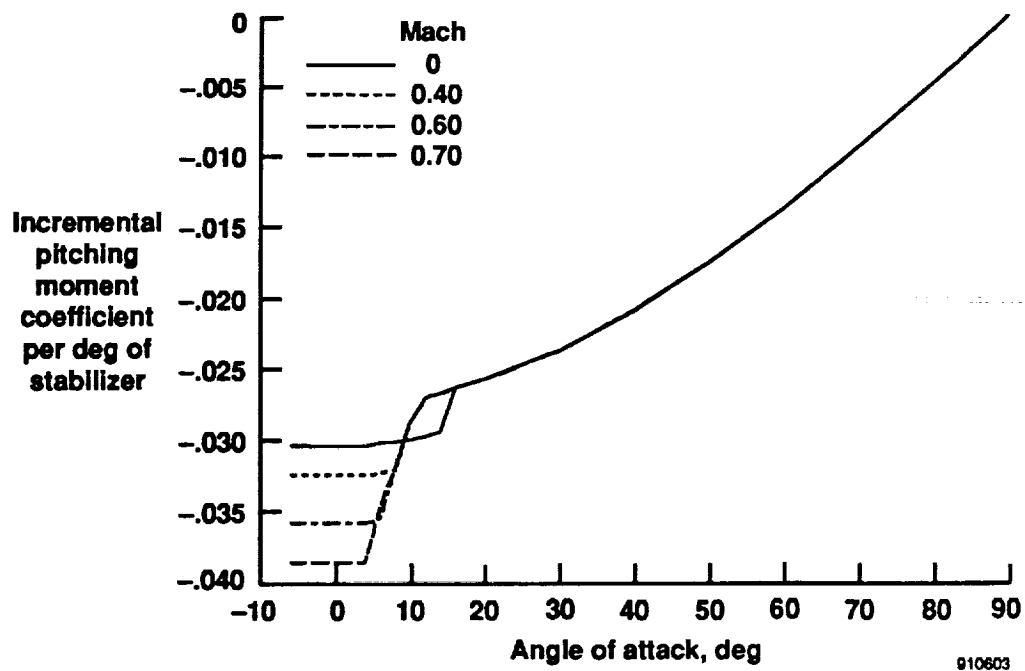
(a) In pitching moment coefficient.
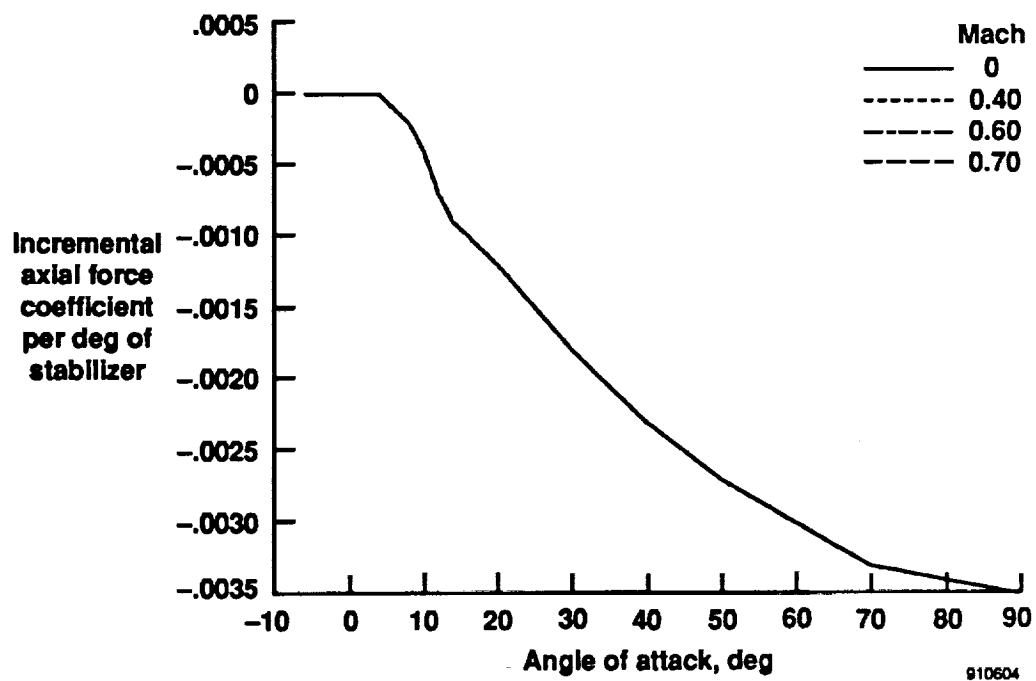


(b) In axial force coefficient.

Figure 14. Stabilizer control effectiveness.

22
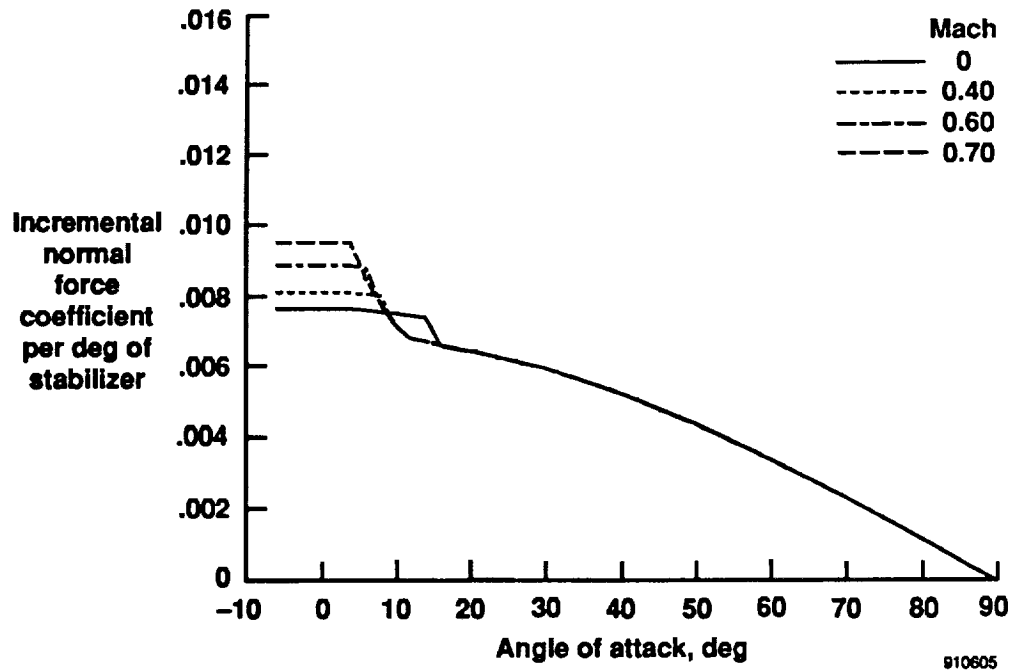
(c) In normal force coefficient.

Figure 14. Concluded.
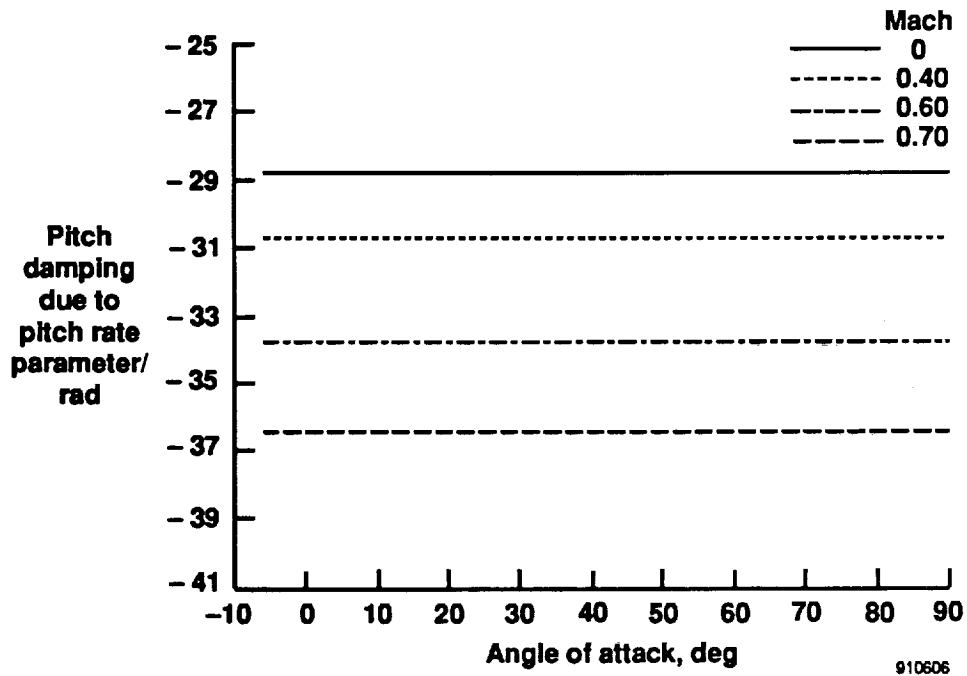


(a) In pitching moment coefficient as a result of pitch rate.

Figure 15. Damping parameter.

23
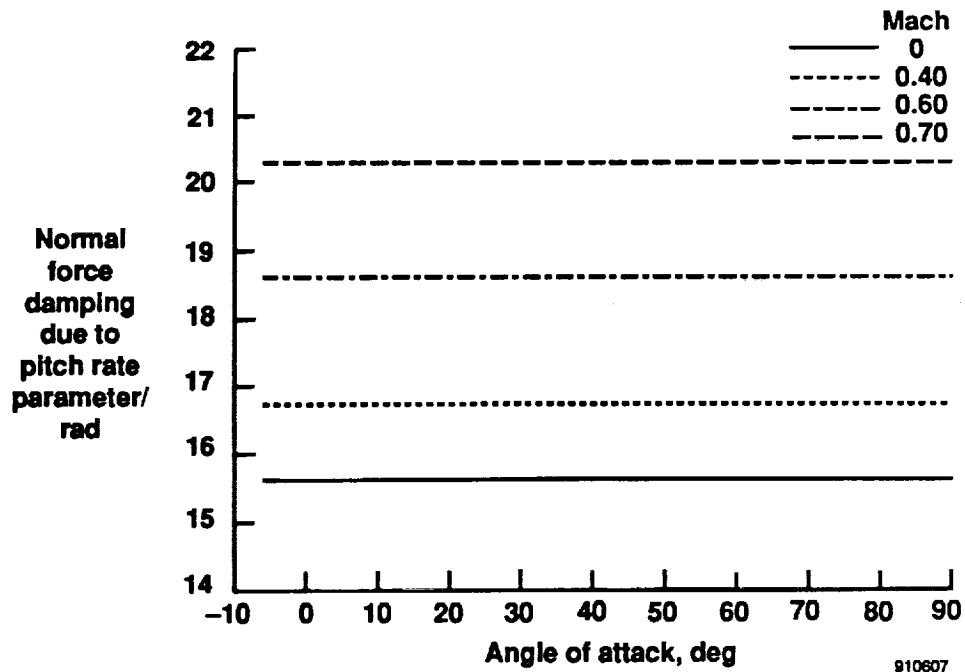
(b) In normal force coefficient as a result of pitch rate.

Figure 15. Concluded.
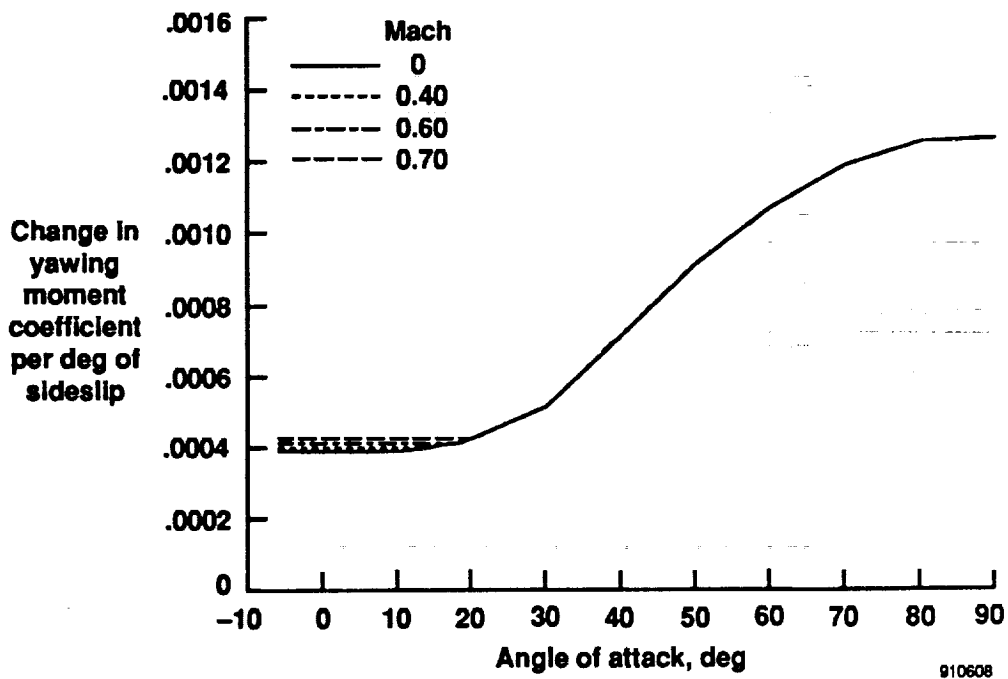


Figure 16. Directional stability derivative.

24
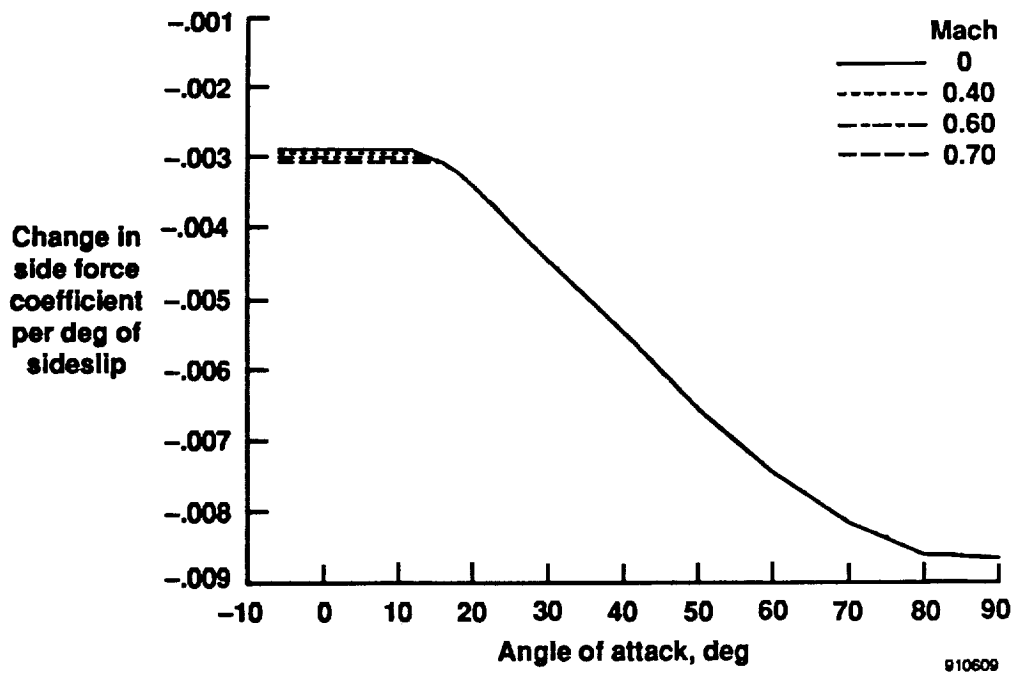
Figure 17. Primary side force stability derivative.
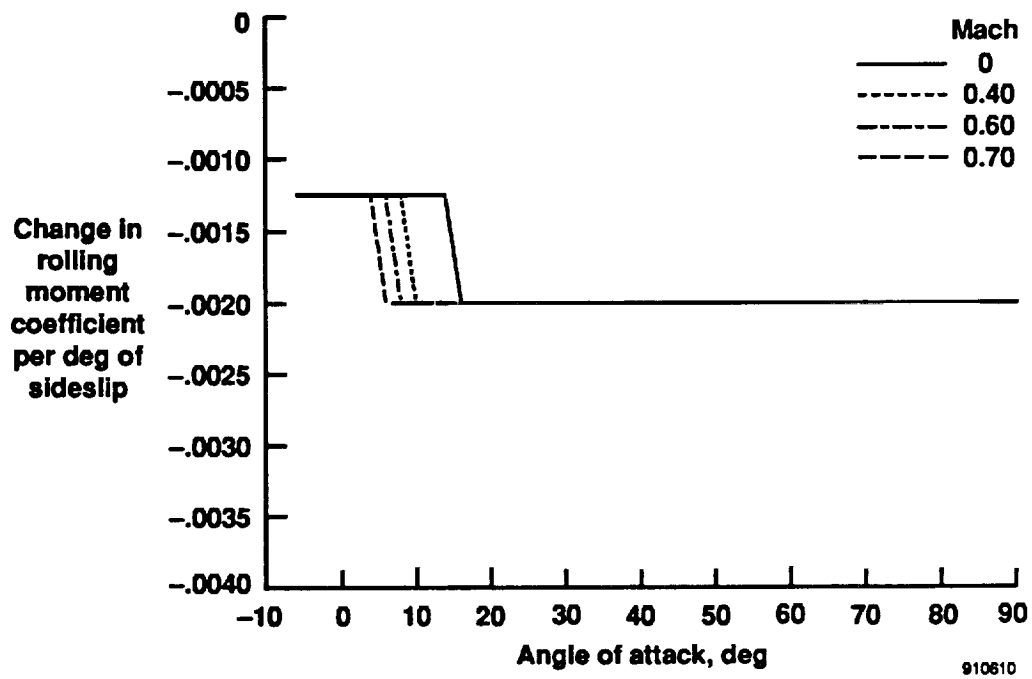


(a) Full calculated value.

Figure 18. Effective dihedral derivative.
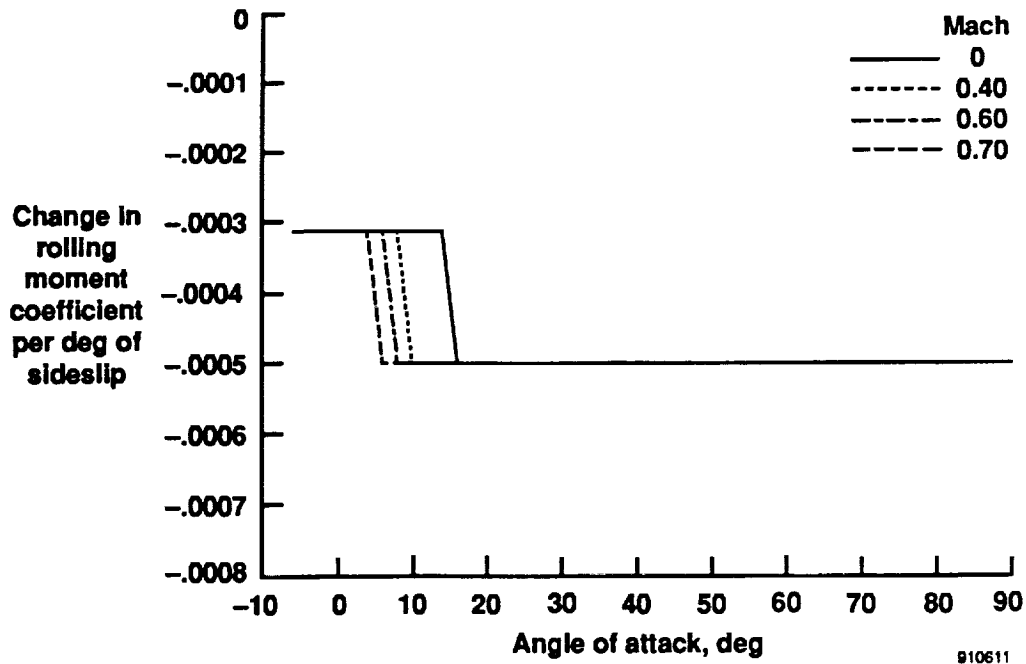
(b) One-fourth of calculated value.

Figure 18. Concluded.
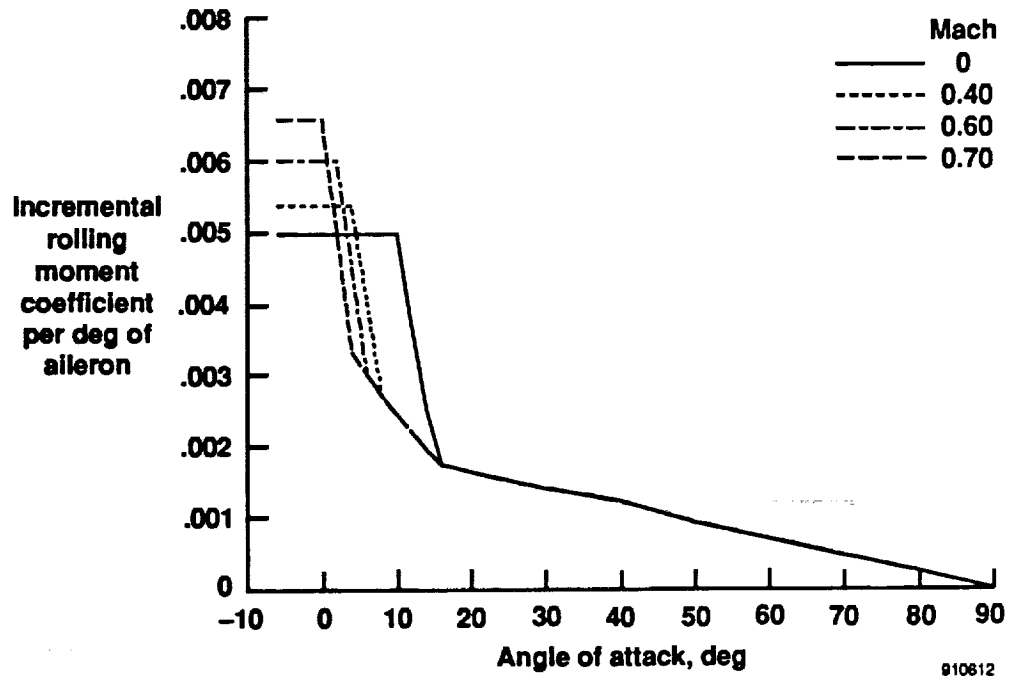


(a) In rolling moment coefficient.

Figure 19. Aileron control effectiveness.

26
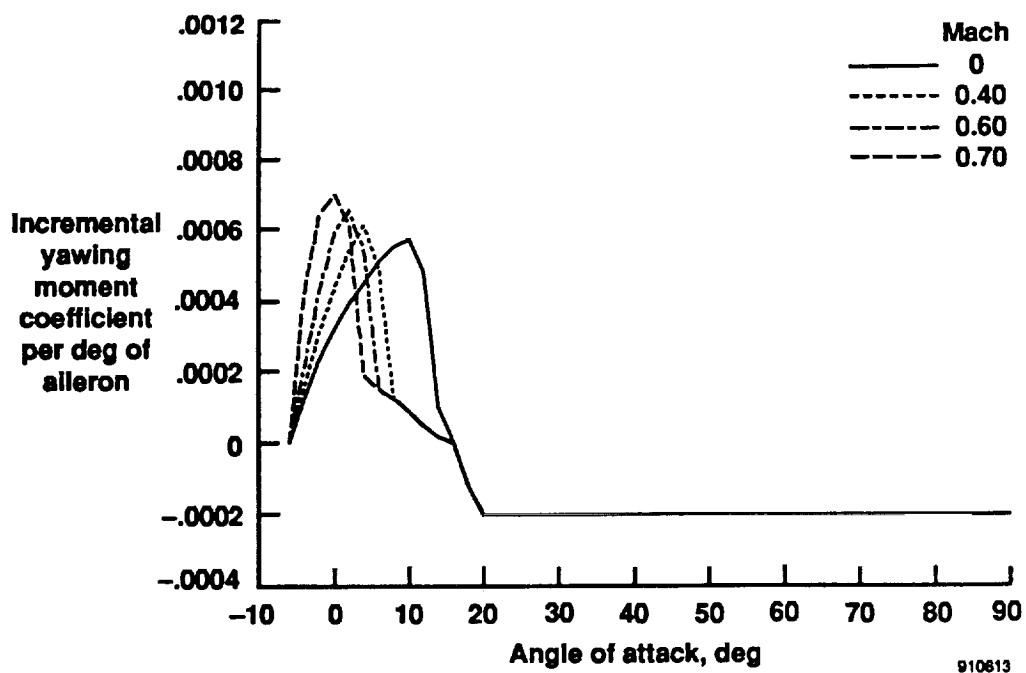
(b) In yawing moment coefficient.
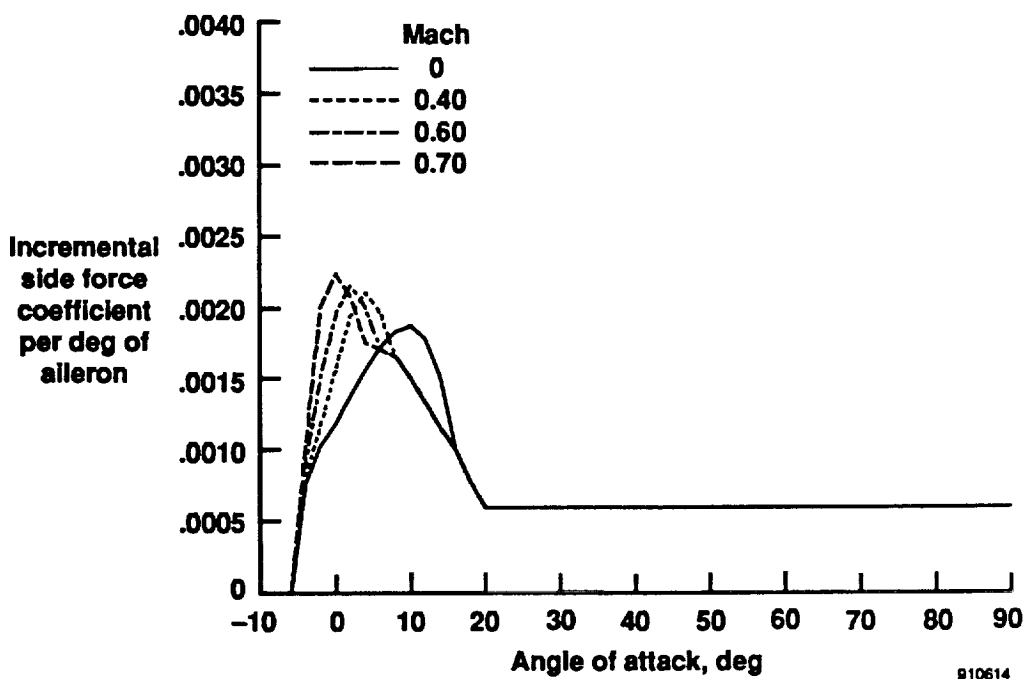


(c) In side force coefficient.

Figure 19. Concluded.

27
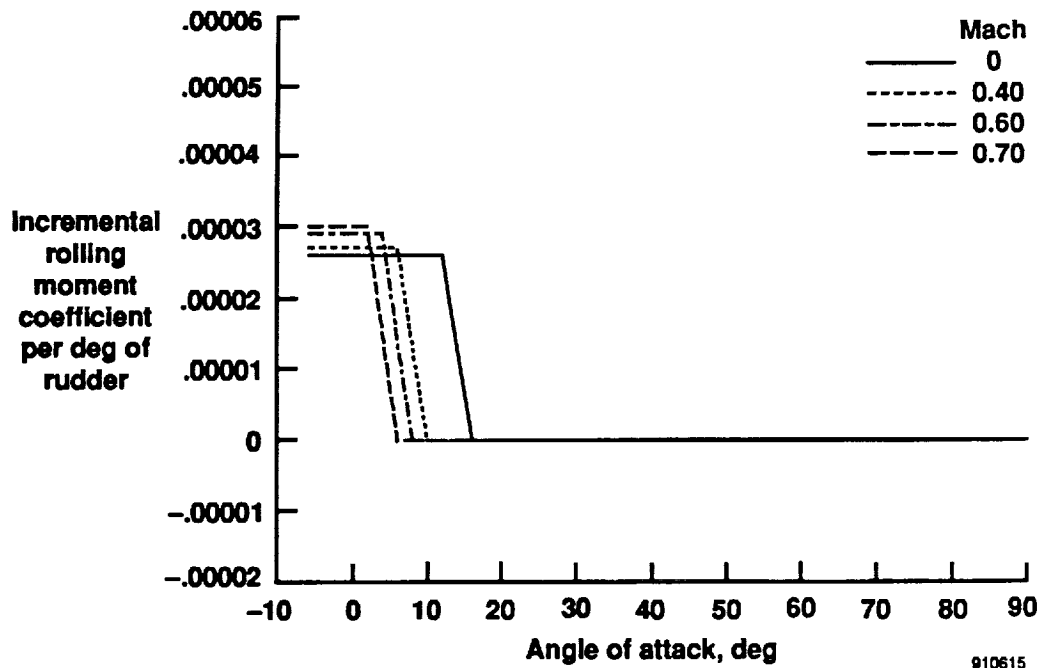
(a) In rolling moment coefficient.
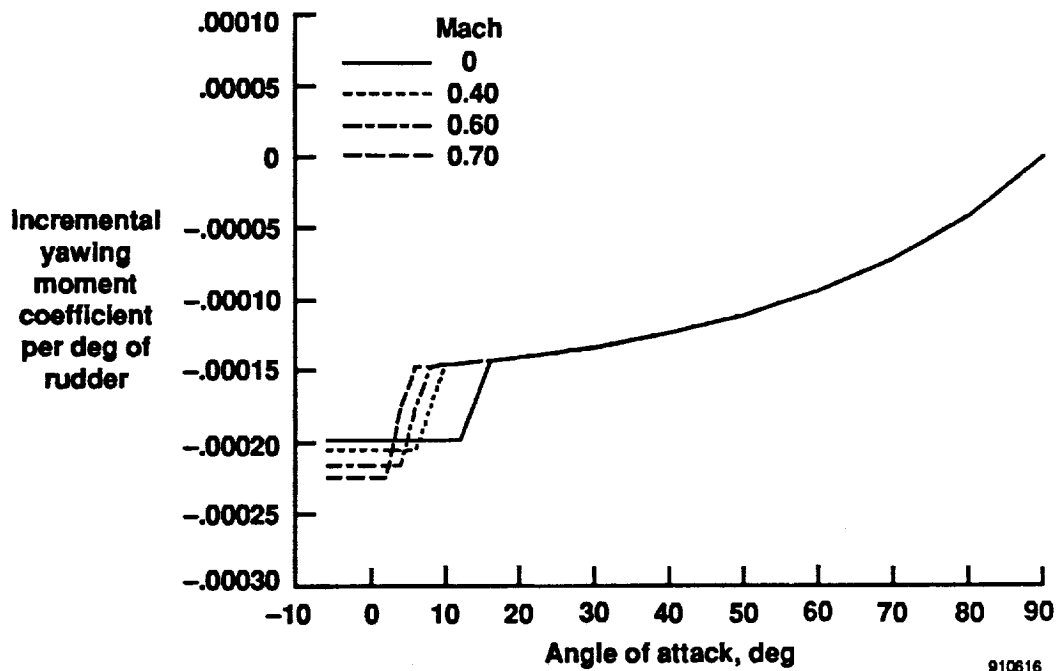


(b) In yawing moment coefficient.

Figure 20. Rudder control effectiveness.

28
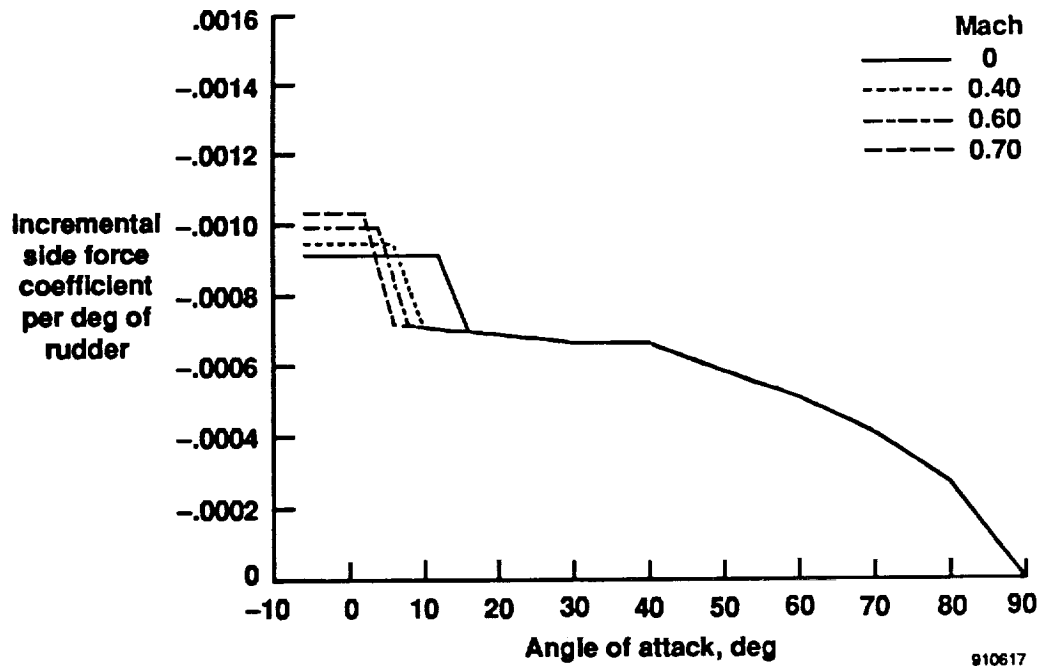
(c) In side force coefficient.

Figure 20. Concluded.
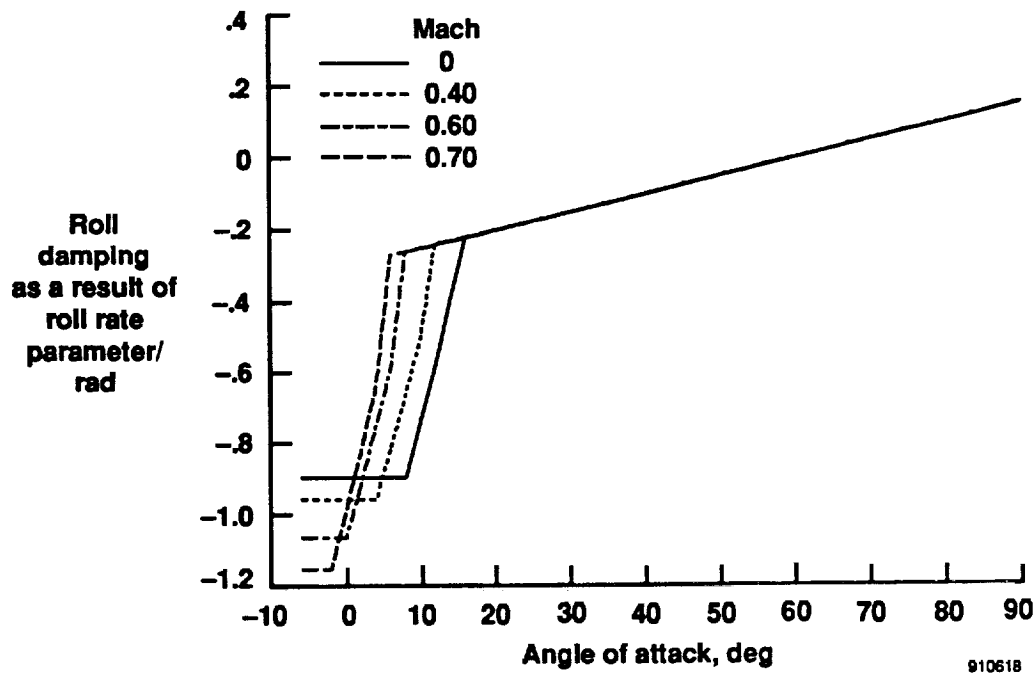


(a) In rolling moment coefficient as a result of roll rate.

Figure 21. Damping parameters.

29
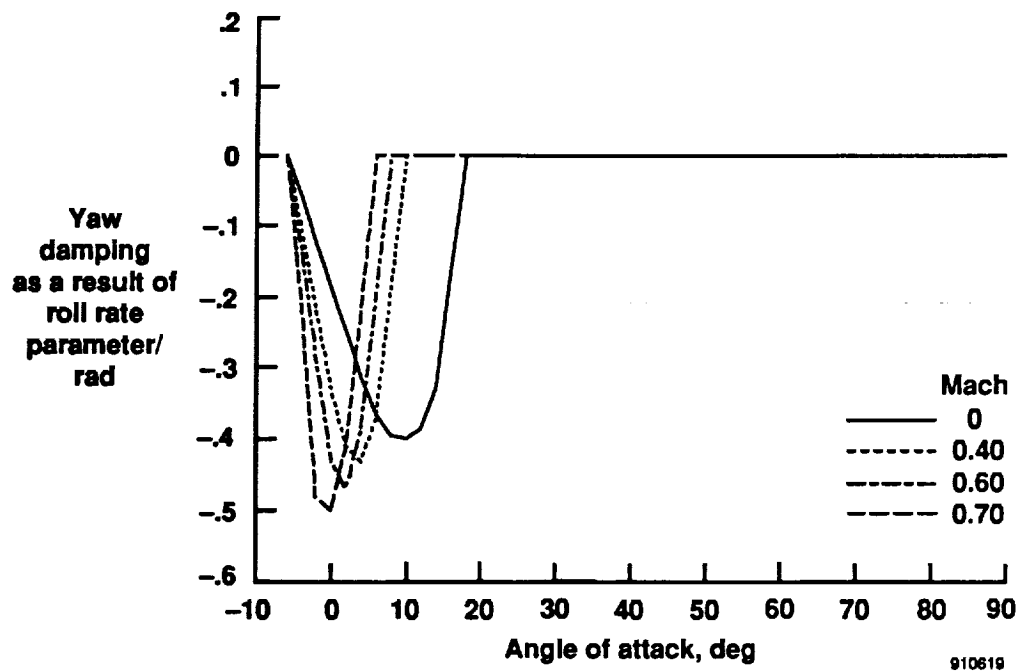
(b)  In yawing moment coefficient as a result of roll rate.
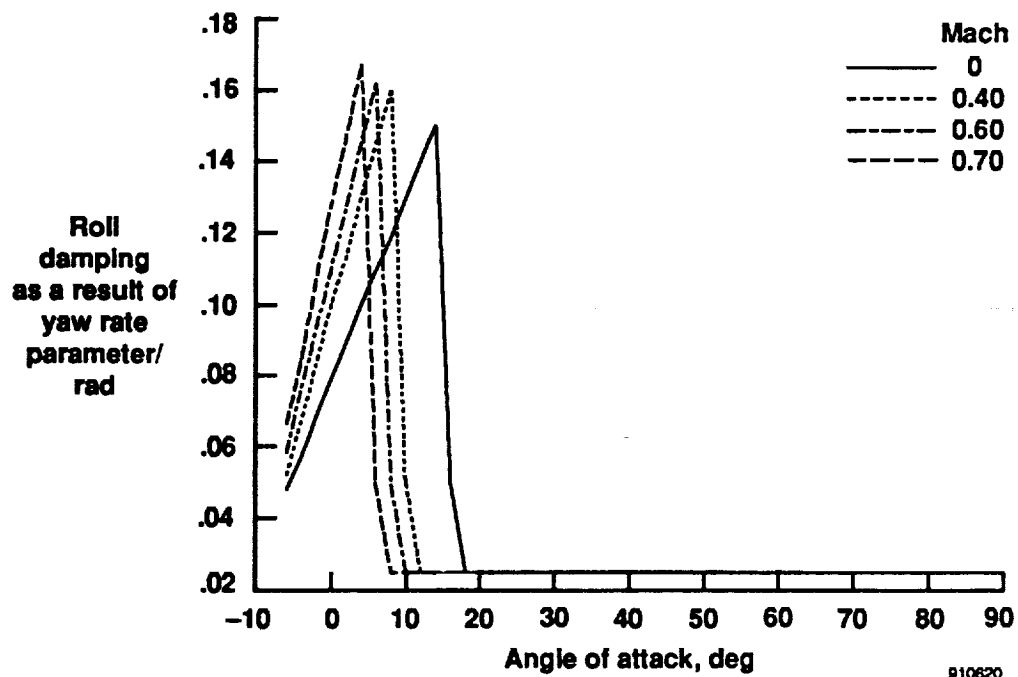


(c)  In rolling moment coefficient as a result of yaw rate.

Figure 21.  Continued.

30
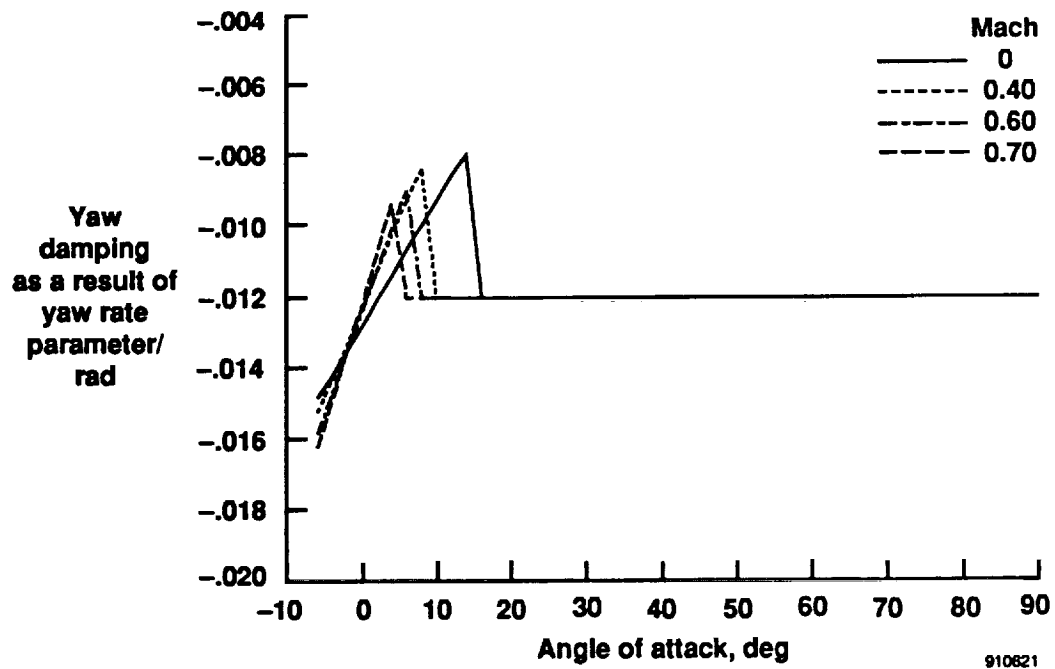
(d) In yawing moment coefficient as a result of yaw rate.

Figure 21. Concluded.
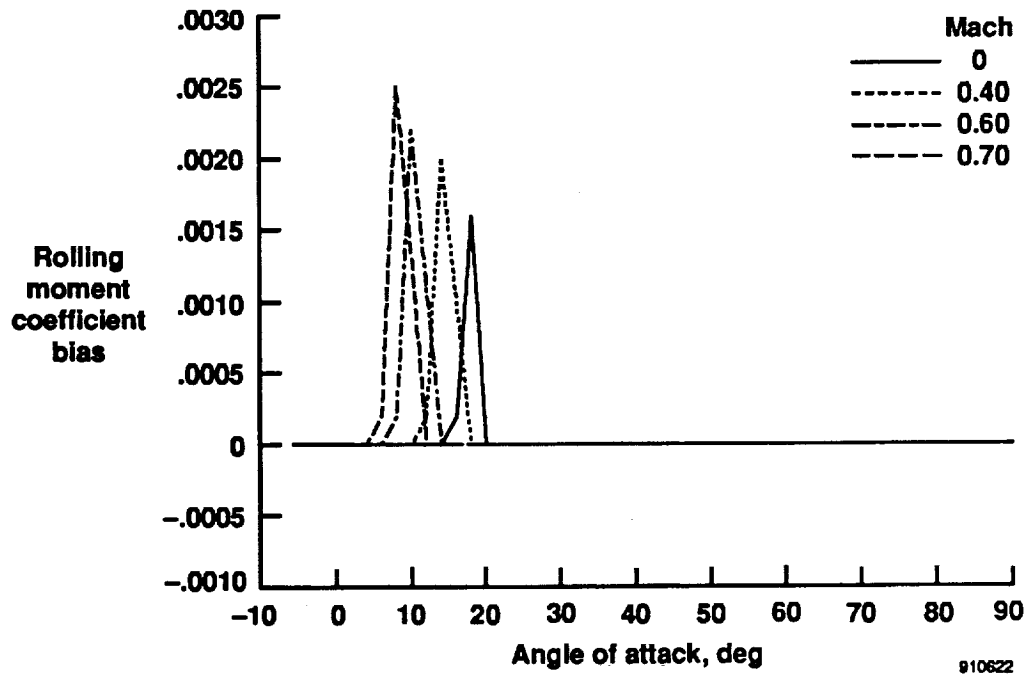


Figure 22. Rolling moment coefficient trim bias.
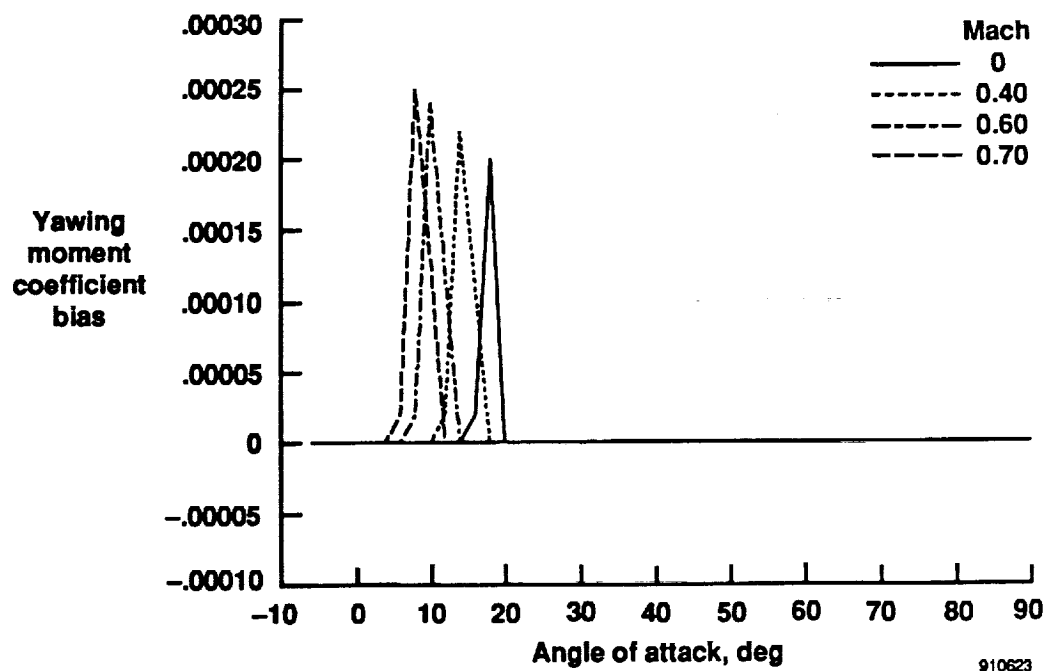
Figure 23. Yawing moment coefficient trim bias.
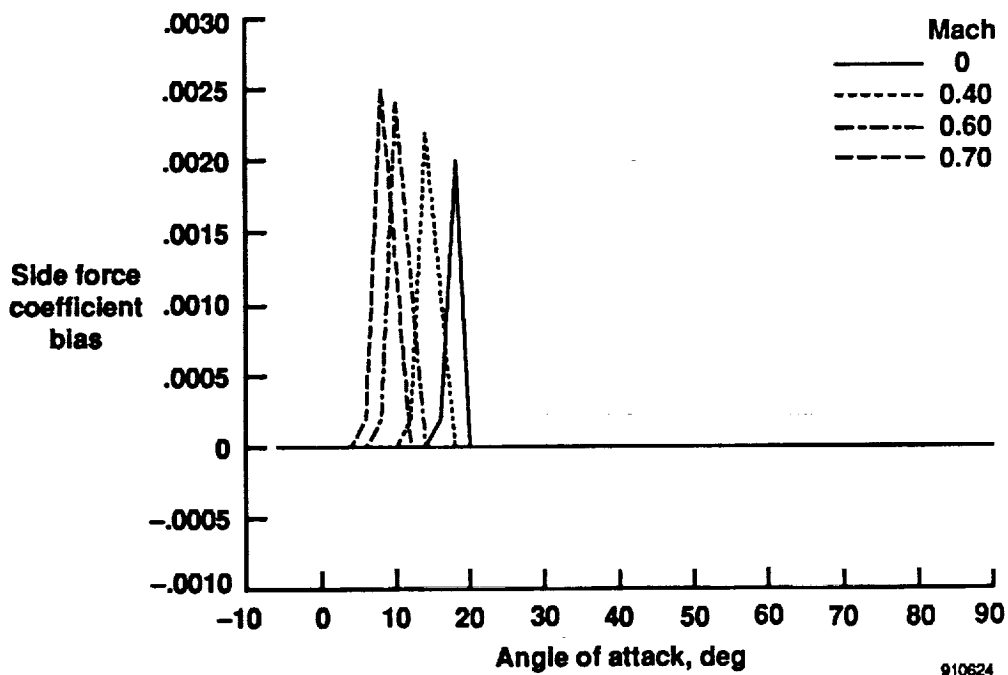


Figure 24. Side force coefficient trim bias.

32
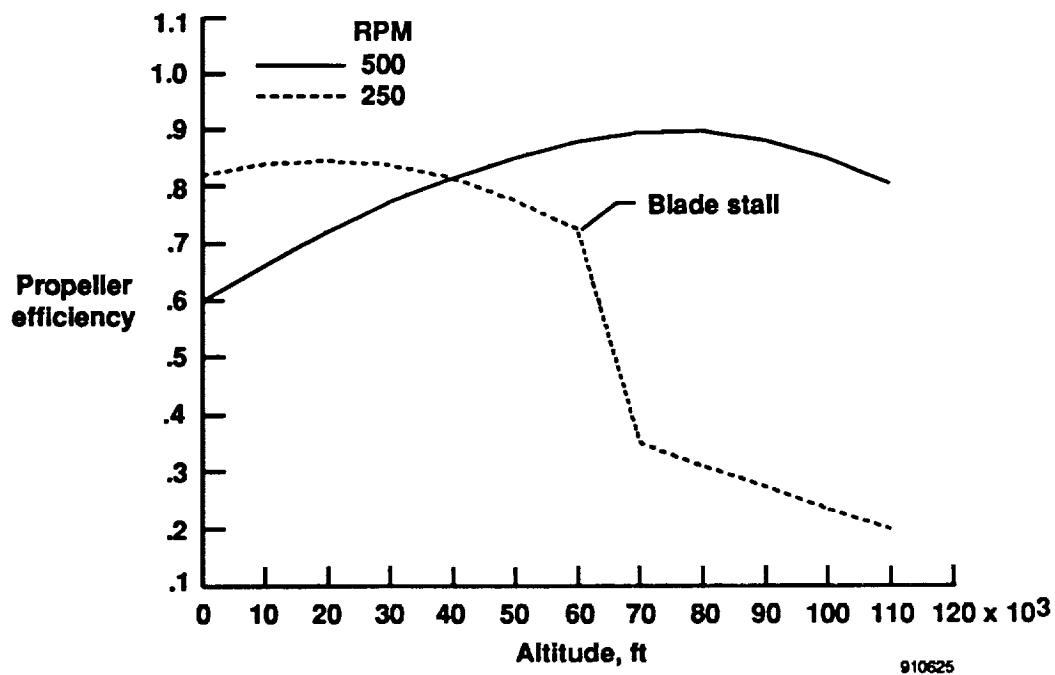
Figure 25. Propeller efficiency.
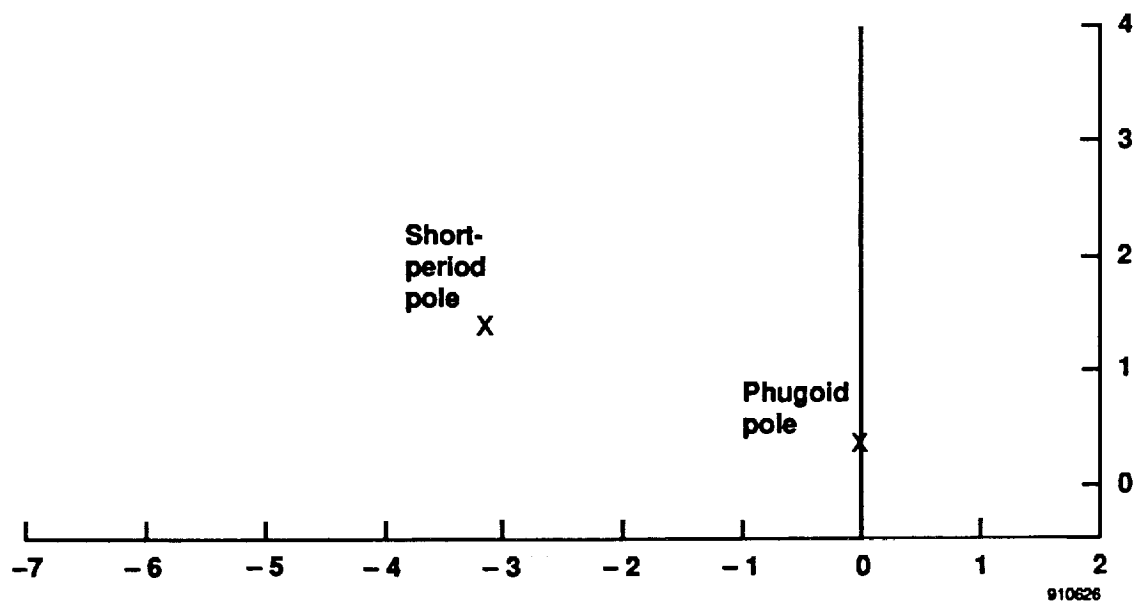


Figure 26. Unaugmented longitudinal eigenvalues for low-altitude flight condition.
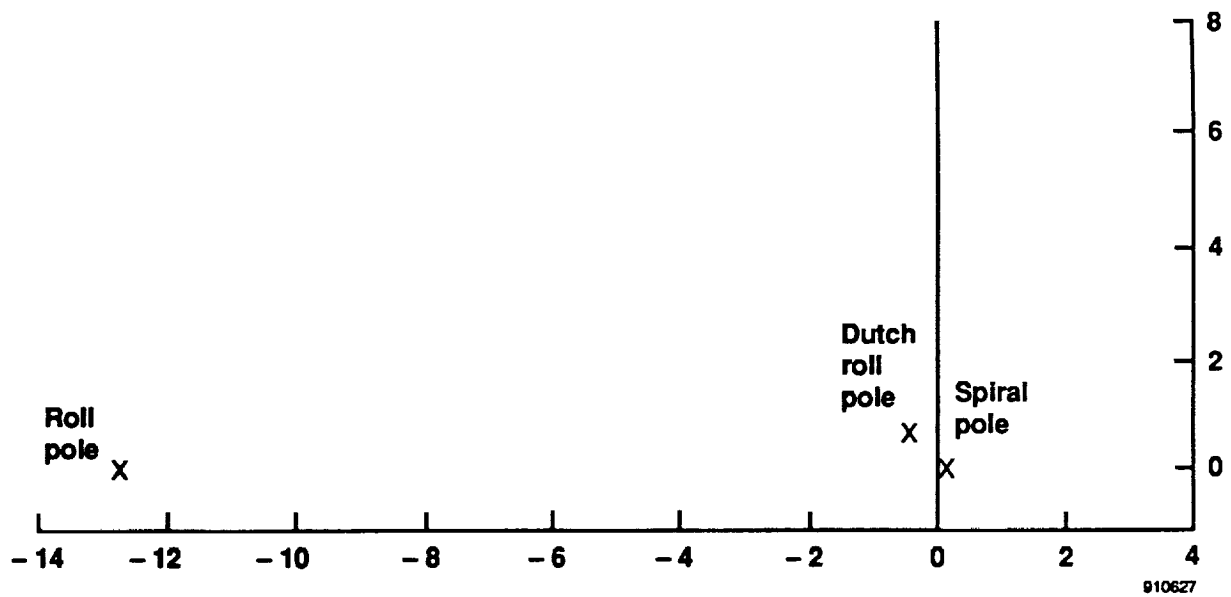
Figure 27. Unaugmented lateral-directional eigenvalues for low-altitude flight condition.
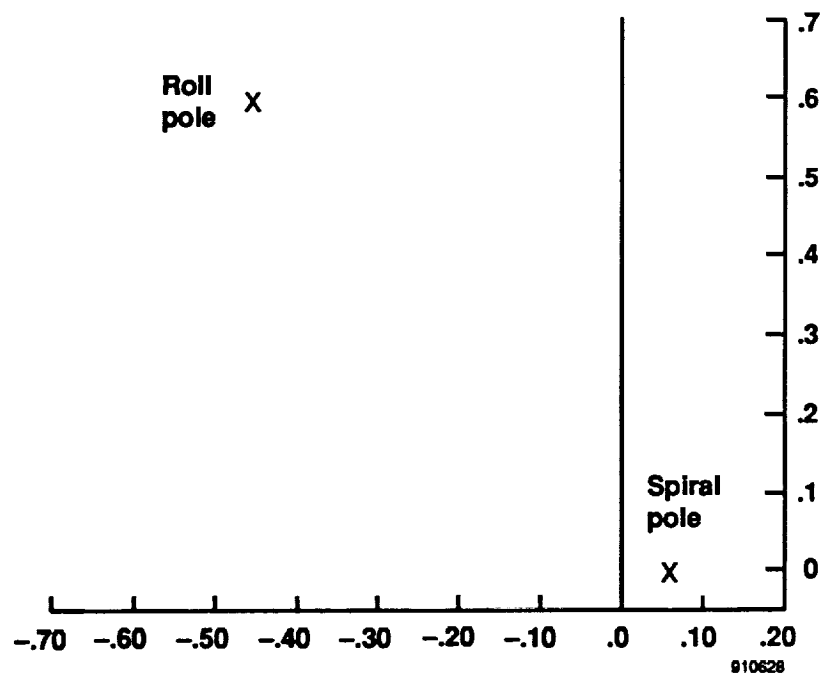


Figure 28. Closeup of unaugmented dutch roll and spiral eigenvalues for low-altitude flight condition.
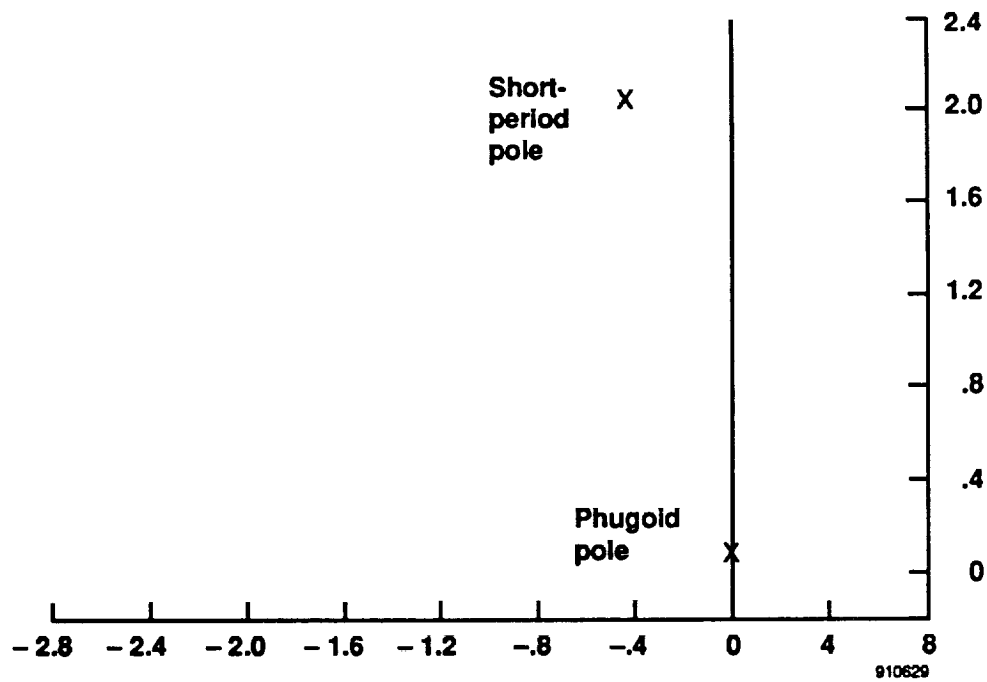
Figure 29. Unaugmented longitudinal eigenvalues for high-altitude flight condition.
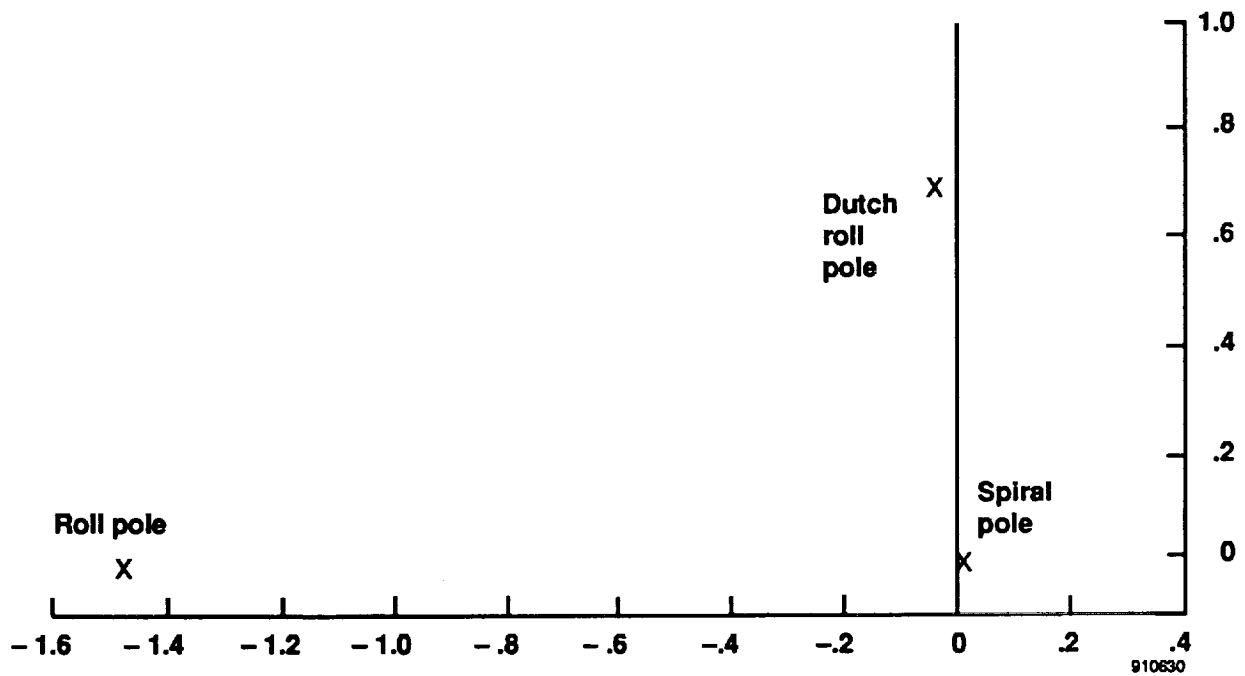


Figure 30. Unaugmented lateral-directional eigenvalues for high-altitude flight condition.
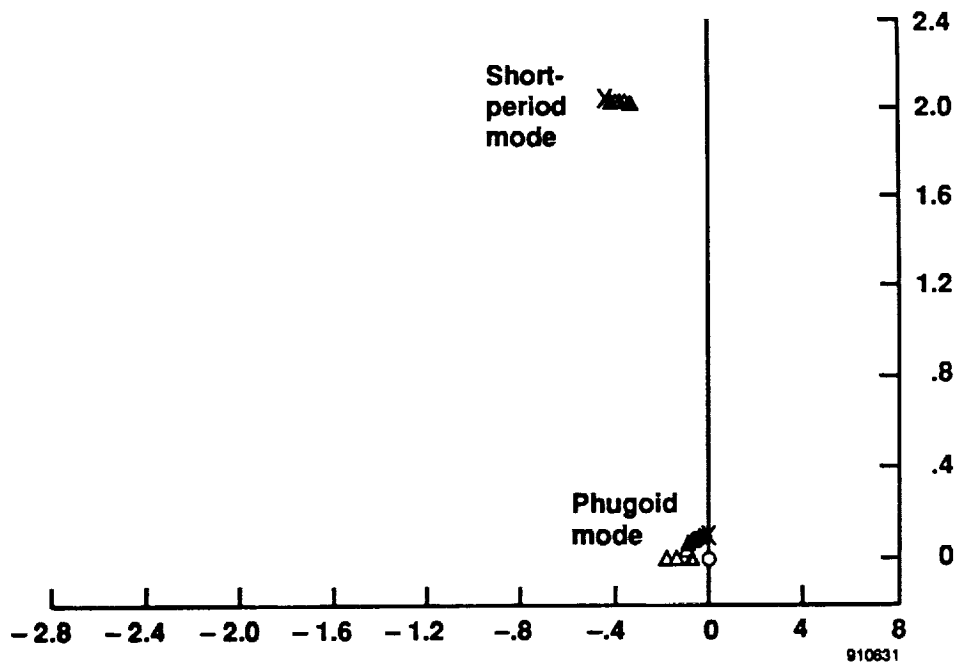
Figure 31. Root loci of flightpath angle to elevator feedback for high-altitude flight condition; gain variation from 0 to 1.0.
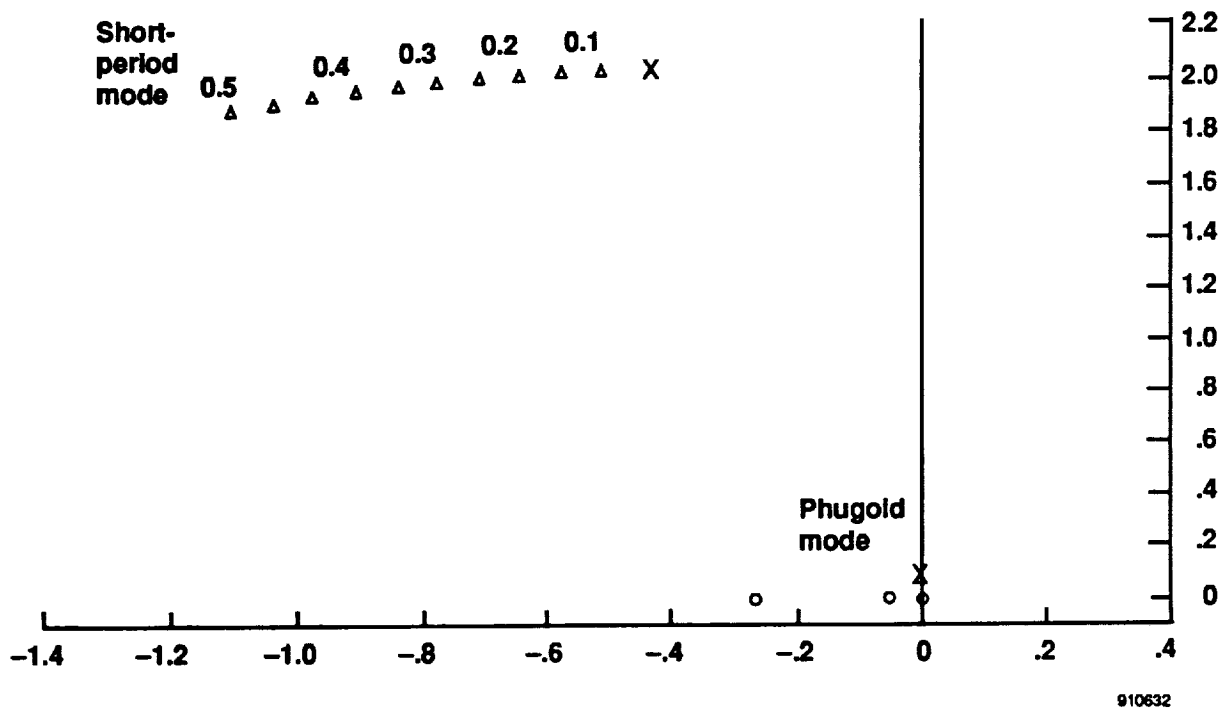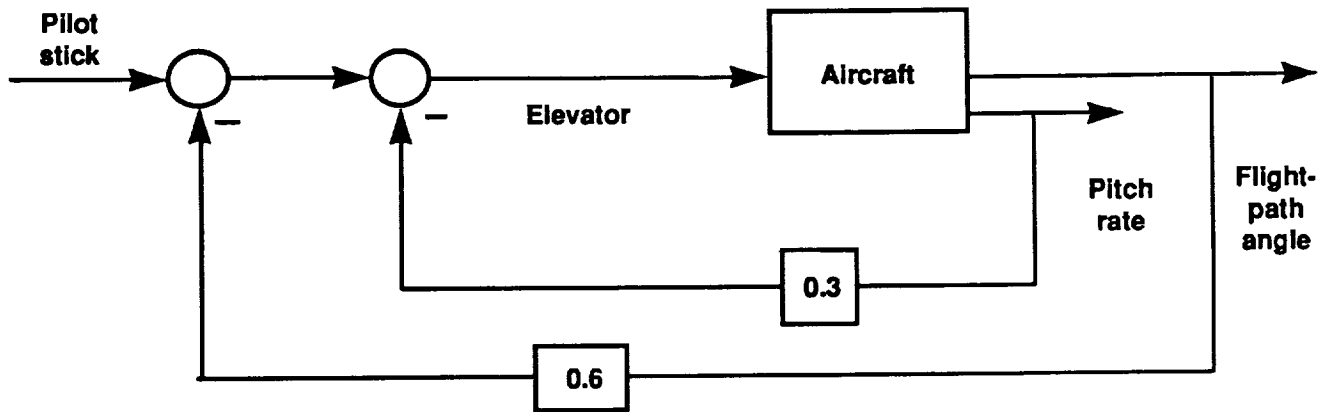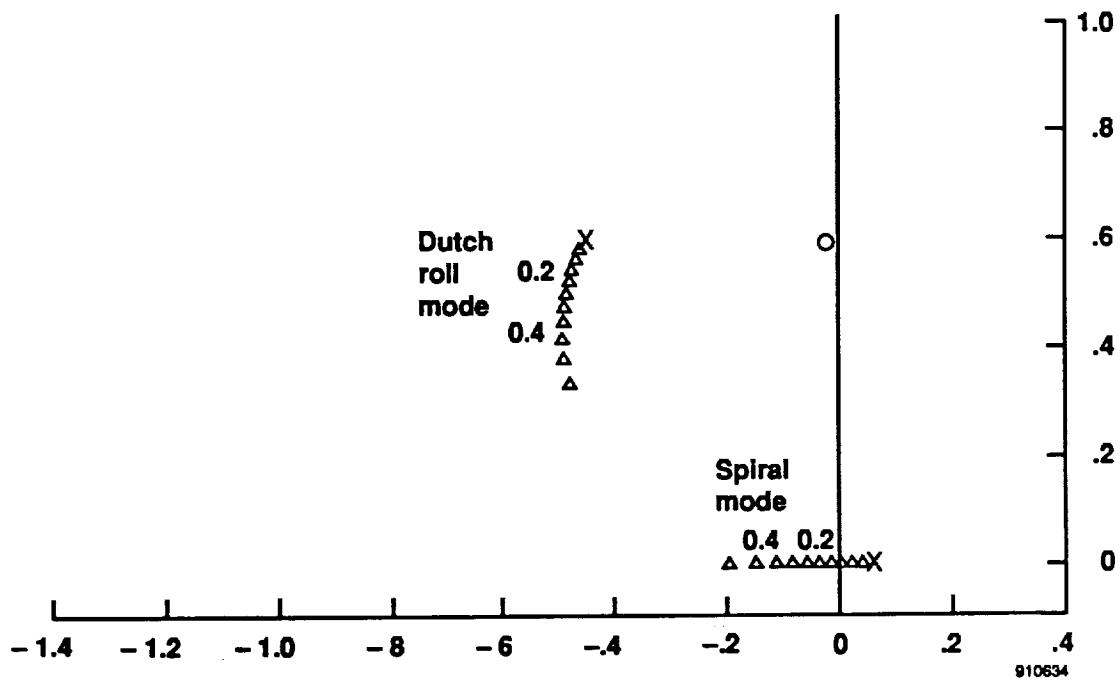


Figure 32. Pitch rate to elevator; gain variation from 0 to 0.5.
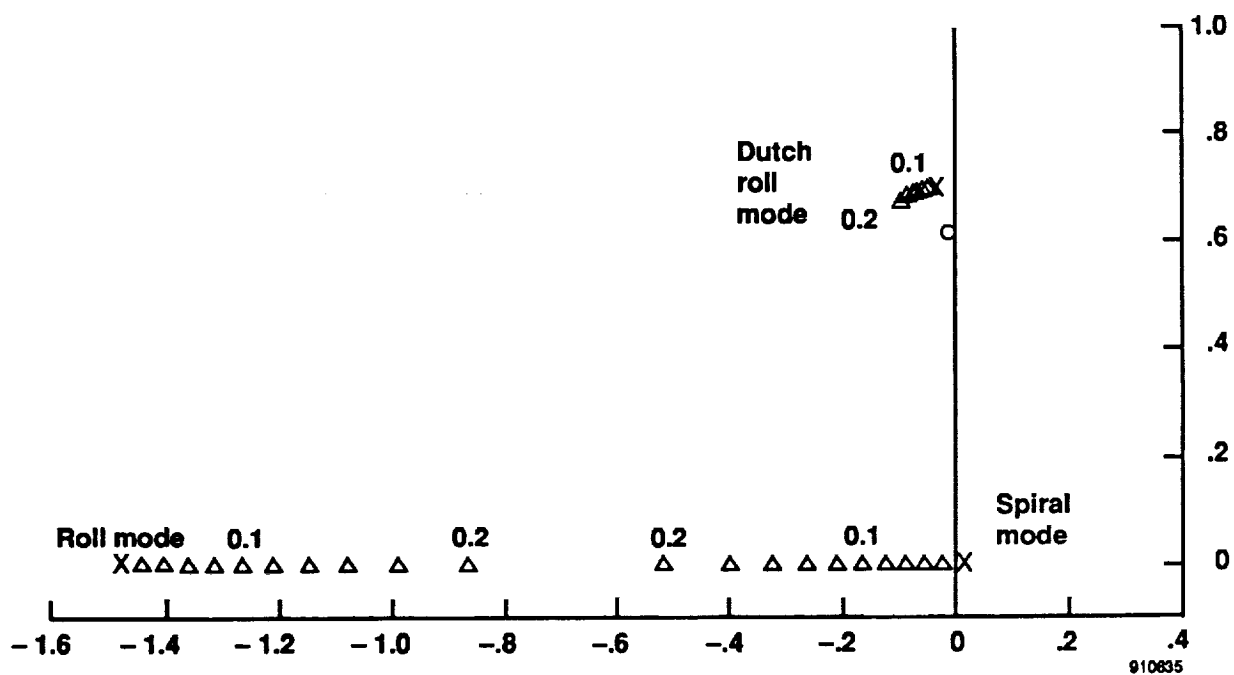
Figure 33. Longitudinal control augmentation with nominal high-altitude gains.



(a) Gain variation from 0 to 0.5; roll mode near −13; low-altitude flight condition.

Figure 34. Root loci of bank angle to aileron feedback.

(b) Gain variation from 0 to 0.2; high-altitude flight condition.
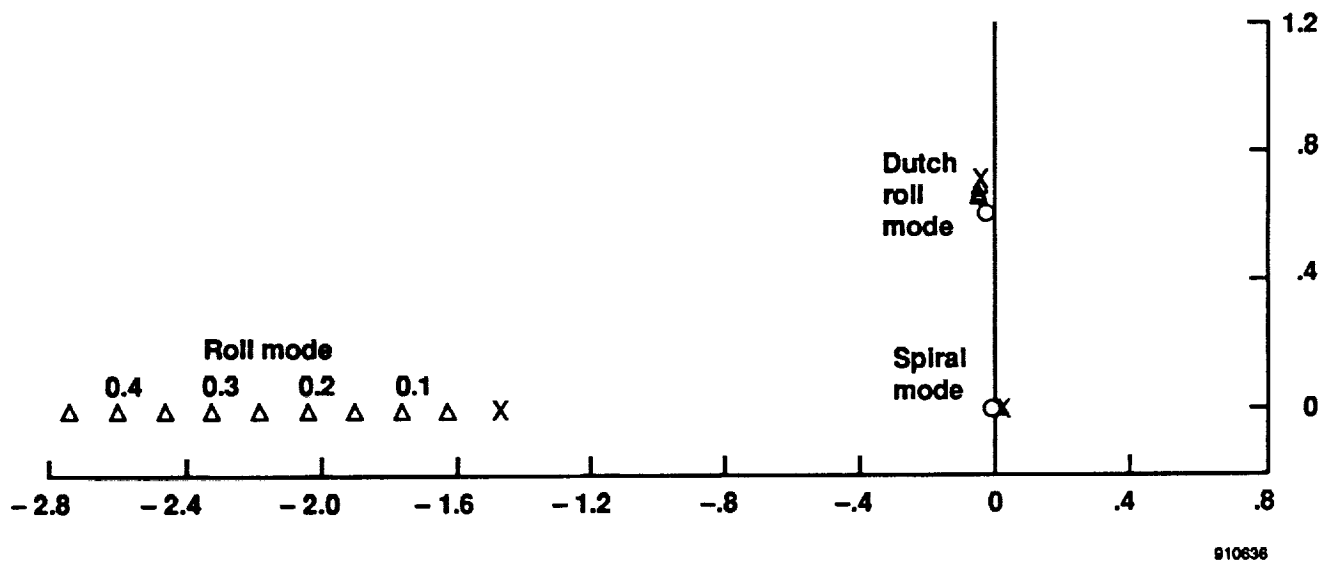
Figure 34. Concluded.



Figure 35. Root loci of roll rate to aileron feedback for high-altitude flight condition; gain variation from 0 to 0.45.
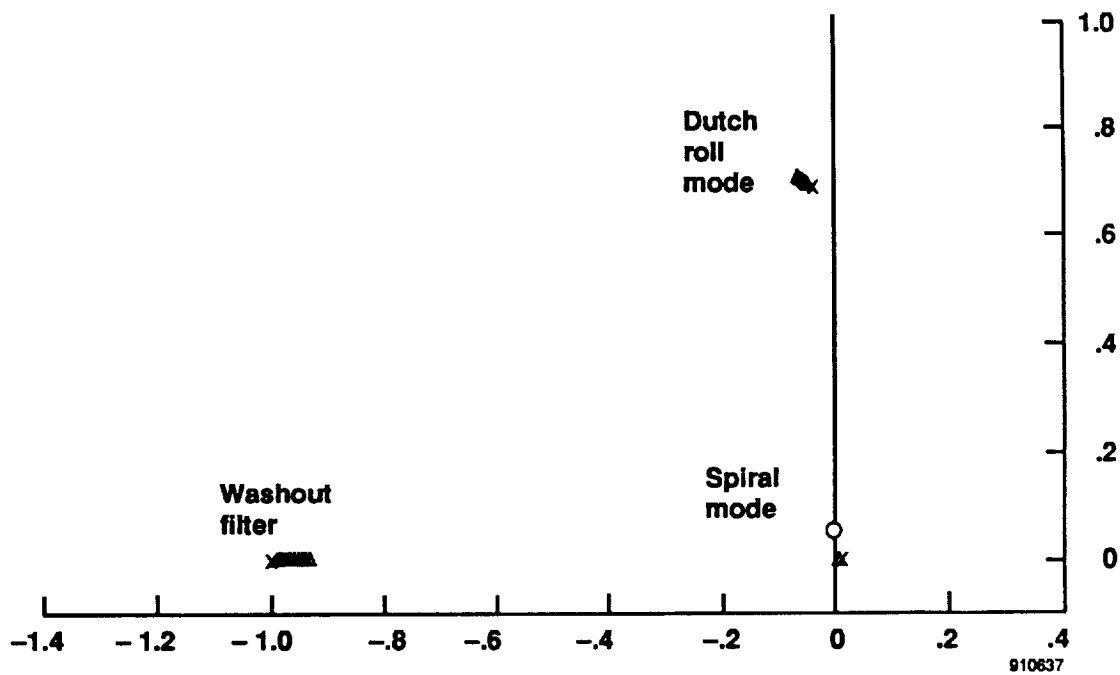
Figure 36. Root loci of yaw rate to rudder feedback for high-altitude flight condition; gain variation from 0 to 0.5; roll mode near 3.46.
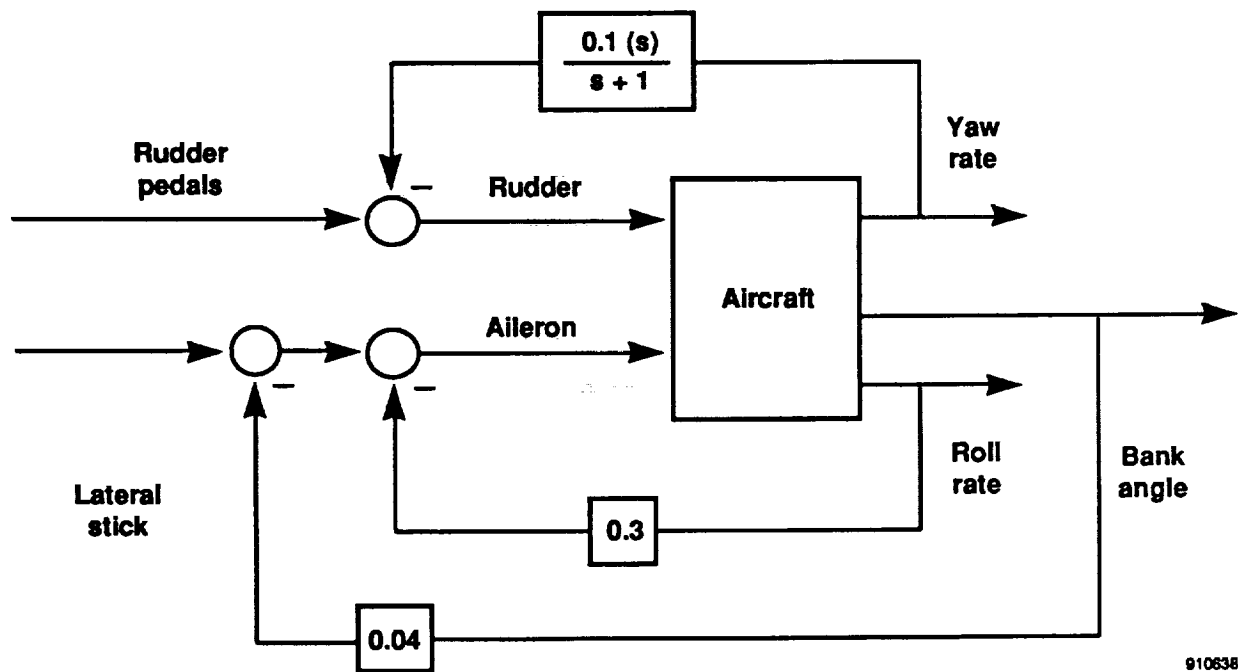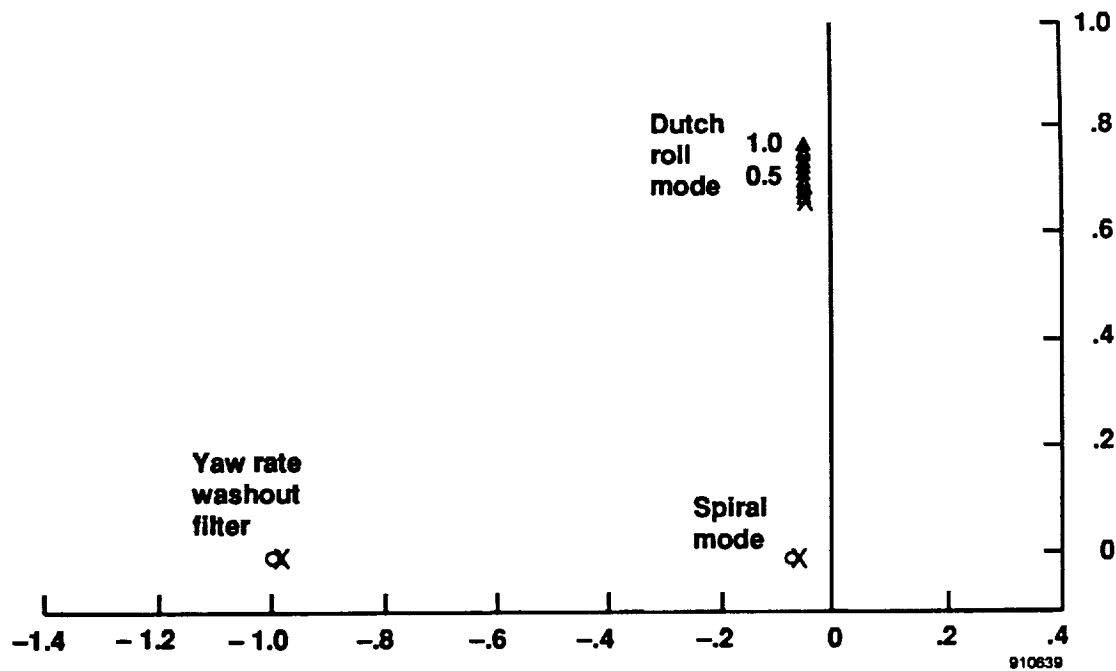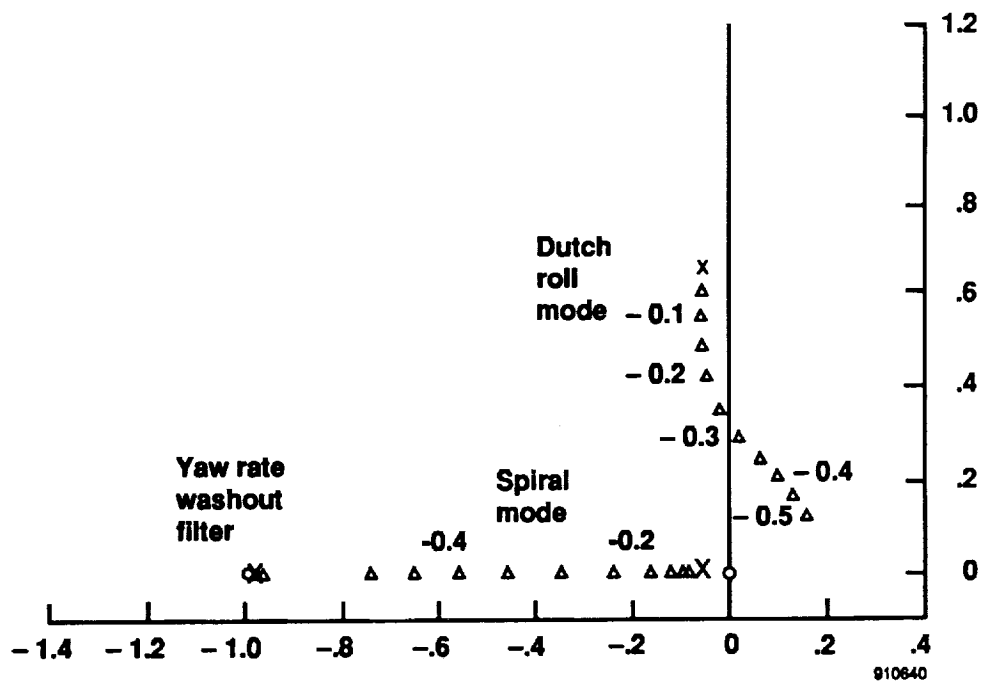


Figure 37. Lateral-directional control augmentation with nominal high-altitude gains.

(a) Root loci of sideslip angle to rudder feedback; gain variation from 0 to 1.0.



(b) Root loci of sideslip angle to aileron; gain variation from 0 to −1.0.

Figure 38. Roll rate, yaw rate, and bank angle loops closed with nominal high-altitude gains for high-altitude flight condition.

# REPORT DOCUMENTATION PAGE

Public reporting burden for this collection of information is estimated to average 1 hour per response, including the time for reviewing instructions, searching existing data sources, gathering and maintaining the data needed, and completing and reviewing the collection of information. Send comments regarding this burden estimate or any other aspect of this collection of information, including suggestions for reducing this burden, to Washington Headquarters Services, Directorate for Information Operations and Reports, 1215 Jefferson Davis Highway, Suite 1204, Arlington, VA 22202-4302, and to the Office of Management and Budget, Paperwork Reduction Project (0704-0188), Washington, DC 20503.

| 1. AGENCY USE ONLY (Leave blank) | 2. REPORT DATE September 1991 | 3. REPORT TYPE AND DATES COVERED Technical Memorandum |
|---|---|---|

**4. TITLE AND SUBTITLE**

Modeling, Simulation, and Flight Characteristics of an Aircraft Designed to Fly at 100,000 Feet

**5. FUNDING NUMBERS**

WU-464-99-01-00

**6. AUTHOR(S)**

Alex G. Sim

**7. PERFORMING ORGANIZATION NAME(S) AND ADDRESS(ES)**

NASA Dryden Flight Research Facility
P.O. Box 273
Edwards, California 93523-0273

**8. PERFORMING ORGANIZATION REPORT NUMBER**

H-1731

**9. SPONSORING/MONITORING AGENCY NAME(S) AND ADDRESS(ES)**

National Aeronautics and Space Administration
Washington, DC 20546-0001

**10. SPONSORING/MONITORING AGENCY REPORT NUMBER**

NASA TM-104236

**11. SUPPLEMENTARY NOTES**

**12a. DISTRIBUTION/AVAILABILITY STATEMENT**

Unclassified — Unlimited
Subject Category 08

**12b. DISTRIBUTION CODE**

**13. ABSTRACT (Maximum 200 words)**

A manned real-time simulation of a conceptual vehicle, the stratoplane, was developed to study problems associated with the flight characteristics of a large, lightweight vehicle. Mathematical models of the aerodynamics, mass properties, and propulsion system were developed in support of the simulation and are presented. The simulation was at first conducted without control augmentation to determine the needs for a control system. The unaugmented flying qualities were dominated by lightly damped dutch roll oscillations. Constant pilot workloads were needed at high altitudes. Control augmentation was investigated using basic feedbacks. For the longitudinal axis, flightpath angle and pitch rate feedback were sufficient to damp the phugoid mode and to provide good flying qualities. In the lateral-directional axis, bank angle, roll rate, and yaw rate feedbacks were sufficient to provide a safe vehicle with acceptable handling qualities. Intentionally stalling the stratoplane to very high angles of attack (deep stall) was investigated as a means to enable safe and rapid descent. It was concluded that the deep-stall maneuver is viable for this class of vehicle.

**14. SUBJECT TERMS**

Deep stall
High-altitude flight
High angle of attack

**15. NUMBER OF PAGES**

44

**16. PRICE CODE**

A03

| 17. SECURITY CLASSIFICATION OF REPORT Unclassified | 18. SECURITY CLASSIFICATION OF THIS PAGE Unclassified | 19. SECURITY CLASSIFICATION OF ABSTRACT | 20. LIMITATION OF ABSTRACT |
|---|---|---|---|